J. Fluid Mech. (1989), *vol.* 209, *pp.* 191–226
Printed in Great Britain

On the dynamics of liquid spreading on solid surfaces

By C. G. NGAN[1] AND E. B. DUSSAN V.[2]

[1] Millipore Corporation, 80 Ashby Road, Bedford, MA 01730, USA
[2] Schlumberger-Doll Research, Old Quarry Road, Ridgefield, CT 06877-4108, USA

(Received 28 October 1988 and in revised form 7 March 1989)

Our main objective is to identify a boundary-value problem capable of describing the dynamics of fluids having moving contact lines. A number of models have been developed over the past decade and a half for describing the dynamics of just such fluid systems. We begin by discussing the deficiencies of the methods used in some of these investigations to evaluate the parameters introduced by their models. In this study we are concerned exclusively with the formulation of a boundary-value problem which can describe the dynamics of the fluids excluding that lying instantaneously in the immediate vicinity of the moving contact line. From this perspective, many of the approaches referred to above are equivalent, that is to say, they give rise to velocity fields with the same asymptotic structure near the moving contact line. Part of our objective is to show that this asymptotic structure has only one parameter. A substantial portion of our investigation is devoted to determining whether or not the velocity field in a particular experiment has this asymptotic structure, and to measuring the value of the parameter.

More specifically, we use the shape of the fluid interface in the vicinity of the moving contact line to identify the asymptotic structure of the dynamics of the fluid. Experiments are performed in which silicone oil displaces air through a gap formed between two parallel narrowly-spaced glass microscope slides sealed along two opposing sides. Since we were unable to make direct measurements of the shape of the fluid interface close to the moving contact line, an indirect procedure has been devised for determining its shape from measurements of the apex height of the meniscus. We find that the deduced fluid interface shape compares well with the asymptotic form identified in the studies referred to above; however, systematic deviations do arise. The origin of these deviations is unclear. They could be attributed to systematic experimental error, or, to the fact that our analysis (valid only for small values of the capillary number) is inadequate at the conditions of our experiments.

1. Introduction

Moving contact lines, the leading edge of a liquid spreading (or receding) across the surface of a solid, are quite common. However, their influence upon the dynamic behaviour of a fluid body can range from significant to ignorable. For this reason we begin in §1.1 with the simple well-known example of the rise of liquid in a vertical capillary to illustrate when and why the materials in the immediate vicinity of the contact line can have a major influence on fluid bodies. However, quantifying this influence under dynamic conditions has proved to be a challenge, the main reason

being that the physics governing the behaviour of the fluids near the contact line is unknown. In §1.2 we discuss the two main approaches which have been pursued over the past fifteen years to model the behaviour of the fluids near the moving contact line. Quantitative comparisons between theory and experiment for one of these approaches, i.e. allowing viscous fluids to slip on the solid surface, are discussed in detail in §1.3. This subsection provides the motivation for the present study. We conclude with a statement of our objectives and a brief description of subsequent sections.

1.1. *The role of the contact angle*

There is little doubt of the importance of the nature of the two immiscible fluids near the contact line under both dynamic and static conditions. The most obvious cases occur when the influence of surface tension cannot be ignored, resulting in the necessity of specifying boundary conditions for the shape of the fluid interface at the contact line.

Under *static* conditions this can be illustrated in a straightforward manner by considering the problem of determining the height of the liquid in a vertical capillary of very small radius, r_c, when its lower end is submerged beneath the horizontal air–liquid interface in a bath of liquid. The pressure field within the liquid, combined with the normal component of the dynamic boundary condition

$$\boldsymbol{n} \cdot \boldsymbol{T}\boldsymbol{n} = \frac{\sigma}{R_m}, \tag{1.1}$$

requires the shape of the interface within the capillary to closely approximate a segment of a sphere, the pressure of the liquid in close proximity to the fluid interface being roughly constant. Here, σ, $\boldsymbol{n}$, R_m and $\boldsymbol{T}$ denote the surface tension, unit outward normal, mean radius of curvature of the fluid interface, and the stress tensor, respectively. The radius of the sphere is determined by the contact angle boundary condition, Θ, its value being a direct consequence of the interactions among the liquid, air and solid in the immediate vicinity of the contact line. If the column of liquid arrives at its final position by rising (descending) through the capillary then the advancing (receding) contact angle, $\Theta_a(\Theta_r)$, should be used. (It is possible to manipulate the system so that any contact angle can be achieved consistent with static conditions, i.e. $\Theta \in [\Theta_r, \Theta_a]$.) Upon balancing the forces exerted on the column of liquid above the surface of the bath, the following expression for the height of rise, H, is obtained

$$H = \frac{2\sigma \cos \Theta}{\rho g r_c},$$

where ρ and g denote the density of the liquid and the gravitational constant, respectively. Hence, the liquid rises to substantial heights, i.e. $H \gg 1$, in systems characterized by very small static contact angles; in systems with static contact angles near 90°, the column of liquid hardly exists at all, $H \approx 0$. Thus, the nature of the materials (the identity of the two fluids, and the finish of the surface of the solid) in the immediate vicinity of the contact line can have a major impact on the macroscopic state of a system through the influence of the contact angle.

Under *dynamic* conditions the situation is similar, although not nearly as straightforward. Upon a cursory inspection of the usual hydrodynamic equations and boundary conditions, it appears that nothing basic has changed. Since the right-hand side of (1.1) remains the same as the static case, retaining the contact-angle

boundary condition at the contact line is justified. However, under dynamic conditions a singularity appears at the moving contact line. Analyses of liquids spreading over solid surfaces are characterized by stress tensors that behave as $1/r$ as r approaches zero when assuming the presence of Newtonian incompressible fluids obeying the no-slip boundary condition at solid surfaces. Here, r denotes the shortest distance to the contact line. Consequently, (1.1) is so singular at the contact line that the contact-angle boundary condition cannot be satisfied; refer to Dussan V. (1979) for a general discussion.† The inadequacy of the usual hydrodynamic assumptions has also been demonstrated through a dimensional analysis of data obtained in an earlier version of the experiments to be presented in this study (Ngan & Dussan V. 1982). There we reported measuring a dependence of h/a (apex height/half gap width) on a and on contact line speed, U, for liquid displacing air between two narrowly spaced parallel plates; however, dimensional analysis based upon the usual hydrodynamic assumptions does not predict a dependence of h/a on a dimensionless parameter containing a for the conditions of the experiment. Thus, both theory and experiment indicate the necessity of an investigation into the nature of the dynamics of the fluids near the moving contact line.

1.2. *Removal of the singularity at the moving contact line*

Generally speaking, studies of the dynamics of the fluids in the immediate vicinity of the moving contact line fall into one of two categories, which can be identified according to the mechanism introduced to eliminate the singularity mentioned above. Either, (i) a very thin film of advancing liquid is assumed to be present over the solid, spreading well ahead of the apparent location of the contact line, or, (ii) both fluids are permitted to slip along the solid wall. The occurrence of the former for specific material systems was first demonstrated by Hardy (1919) by investigating the behaviour of drops of acetic acid placed on glass in a dry air environment. The detection of the film consisted of measuring the static friction of the surface of the glass. Since then, more sophisticated techniques have been used such as interferometry and ellipsometry to probe the shapes of these films (Bascom, Cottington & Singleterry 1964; Ausserre, Picard & Leger 1986). Theoretical studies of the dynamics of the liquid within these films consist of including long-range intermolecular forces in the form of a disjoining pressure in the Navier–Stokes equation (refer to the review by de Gennes 1985). However, the inclusion of conservative body forces alone in the Navier–Stokes equation cannot eliminate the singularity (Dussan V. & Davis 1974); it merely shifts its location to the moving contact line situated at the leading edge of the precursor film. *Ad hoc* assumptions must still be made about the dynamics of the fluid at the leading edge of the precursor film in order to completely describe the spreading of liquids on solid surfaces. This latter point has not received much attention.

The other approach to remove the singularity, permitting the viscous fluids to undergo a substantial amount of slip along the surface of the solid in the immediate vicinity of the moving contact line, in our opinion has been motivated as much by its mathematical simplicity as by its physical relevance. Over the years a variety of slip boundary conditions have been used, the most popular being the one introduced by Navier in 1823

$$\boldsymbol{\tau} \cdot \boldsymbol{T}\boldsymbol{n} = \beta \boldsymbol{\tau} \cdot \boldsymbol{u}. \tag{1.2}$$

† The claim of Pismen & Nir (1982) that an ignorable singularity can arise when $\Theta_s = \pi$ has been shown to be erroneous (Ngan & Dussan V. 1984).

Here, $\boldsymbol{n}$ denotes the unit outward normal to the solid; $\boldsymbol{\tau}$ is defined to be $\boldsymbol{u}/|\boldsymbol{u}|$; β, a constant, is often referred to as the *slip coefficient*. Goldstein (1938) points out that in the nineteenth century, when the appropriate boundary conditions for the then newly formulated Navier–Stokes equation were being identified, logic dictated that the boundary condition between a viscous fluid and solid should reflect, in part, the chemical composition of the fluid and the solid, as well as the roughness of the solid surface. The no-slip boundary condition was gradually adopted only after much debate, the justification being the accuracy to which it predicts experimentally observed laminar flow regardless of the identity of the materials and the finish of the solid surface. The most notable exception, as demonstrated by Maxwell, occurs for rarefied gases, in which case (1.2) is in agreement with experiments.

Goldstein (1938) considers only one-component fluid systems. Apparently, the appropriate boundary condition for a multi-component (miscible) fluid system is as yet not known. Jackson (1977) points out in a review restricted to viscous gases that using the no-slip boundary condition on the mass averaged velocity, the velocity appearing in the Navier–Stokes equation, can lead to substantial error.

Richardson (1973) gives some insight into the success enjoyed by the no-slip boundary condition through an analysis of the influence of roughness of the solid surface on the velocity field. The roughness was idealized by a one-dimensional periodic structure. Although he applies the shear-free boundary condition to the fluid–solid boundary, the velocity field generated away from the solid corresponds to that of a fluid obeying the no-slip boundary condition. Recently, Jansons (1988) has examined the effect of a sparse randomly roughened solid surface, thus removing the necessity of assuming a highly idealized structure at the solid surface. His results indicate that random structures are more effective than one-dimensional periodic structures in generating an apparent no-slip boundary condition.

Hocking (1976), motivated by a desire to derive an expression for β appropriate for systems containing moving contact lines, extended Richardson's model (although their analyses differ quite a bit) to include the presence of a second immiscible fluid (gas or liquid) within the troughs of the one-dimensional periodic structure on the surface of the solid. This he assumes corresponds to the state of the surface downstream from the contact line when some of the receding fluid fails to be removed. However, the derivation presumes that the lengthscale associated with the velocity field is large compared to the periodic structure modelling the roughness, a condition violated in the immediate vicinity of the moving contact line when (1.2) is used as a boundary condition (Hocking 1977; Huh & Mason 1977). (Hocking (1977), Richardson (1973) and Jansons (1988) assume in their analyses that the velocity approaches a constant, unidirectional, translationally invariant shear away from the solid. Presumably, this limits the use of their derivations of β to situations having, at most, small changes in velocity along the solid surface.) Other shortcomings exist, as pointed out by Hocking, e.g. not taking into account the inherent unsteadiness of the velocity field associated with contact lines moving over rough surfaces, especially when the surfaces contain grooves with sharp edges, as do some of Hocking's models. This latter point has been pursued by Jansons (1986). His calculations indicate that locally unsteady motion at the moving contact line owing to surface roughness justifies the use of a slip boundary condition with a velocity dependent slip length, its size being larger than the scale of the roughness.

1.3. *Quantitative comparisons between experiment and theory assuming the fluid slips at the solid surface*

Despite the lack of physical justification, Navier's boundary condition has been used to analyse fluid mechanics problems containing moving contact lines (Hocking 1976, 1977; Huh & Mason 1977; Lowndes 1980; Hocking 1981; Hocking & Rivers 1982; Hocking 1983; Bach & Hassager 1985). These include immiscible fluid displacement through capillaries and between two parallel plates, drops spreading symmetrically on a horizontal surface, and the steady motion of a two-dimensional drop down an inclined plane. In each case, values must be specified for *two* parameters arising from the model at the moving contact line: the contact angle, Θ, and the slip coefficient, β.

The most desirable approach for obtaining values of the contact angle would be by direct measurement under relevant dynamic conditions for the particular material systems of interest. However, the theoretical analyses indicate a rapidly changing interfacial slope within very small distances of the moving contact line. Thus measurements of the shape of the fluid interface would have to be made on the slip lengthscale, L_s, (defined as $2\mu/\beta$, μ denoting the dynamic viscosity of the fluid)† in order to determine the value of the contact angle. Since those analyses whose results have been compared with experiments use values for the slip length – usually rationalized to be close to the molecular lengthscale – of 10^{-7} cm (Huh & Mason, Lowndes), 10^{-7} to 10^{-5} cm (Hocking & Rivers), and 10^{-5} cm (Cox 1986), the shape of the fluid interface would have to be scrutinized on the submicrometre lengthscale in order to be able to extract the value of the contact angle. This makes an experimental determination of the contact angle under dynamic conditions infeasible with an optical microscope. Since dynamic contact angles on such small lengthscales have not been measured, assumptions must be made. By far and away, the most common assumption has been that the contact angle is always equal to its static advancing value, Θ_a (all of the experiments involved advancing liquids). The degree of agreement between theoretical predictions and experimental measurements is usually cited as evidence justifying this approach.

Even if there were no systematic deviations between the experimental data and the theoretical predictions, it would still be appropriate to examine the procedure by which theory and experiment are compared. As noted above, the dynamic contact angle in all of these studies is assumed to be Θ_a, the static advancing angle. The criterion employed by Huh and Mason, Lowndes, and Cox for determining the value of the slip coefficient consists of requiring the theoretically predicted value of the apparent contact angle to coincide with its experimentally measured value. The fact that the same value of the slip coefficient can be used over a range of contact line speeds is cited as evidence establishing agreement between theory and experiment. However, the conclusiveness of this line of reasoning is not at all obvious. At every contact line speed there are two unknowns, the contact angle and the slip coefficient. Hence, the necessity for two measurements at every contact line speed seems apparent. It is only after having determined the values of the contact angle and the slip coefficient at every speed of interest that one is in a position to assess the degree to which they depend on the speed of the contact line.

† Although Bach & Hassager strongly imply in their introduction that they use (1.2), an explicit equation containing their slip coefficient is never given. Elsewhere, refer to the top of p. 178 and to p. 181, statements are made implying the implementation of a slip condition only *at* the contact line.

Bach & Hassager, in fact, determine the contact angle and slip coefficient from two experimental measurements. Specifically, they restrict their attention to one particular contact line speed and use the apparent contact angles measured at two different plate separations in an earlier set of experiments reported by us (Ngan & Dussan V. 1982). They find that using a contact angle of 35° and a slip length of 2.8×10^{-4} cm (obtained by multiplying their slip number, Bs, by a, the half gap width) gives rise to apparent contact angles of 54° and 63° for half gap widths of 0.005 cm and 0.035 cm, respectively, for silicone oil (10 poise) displacing air from glass at a contact line speed of 0.04 cm/s. These angles are within $\pm 1.5°$ of the experimentally reported values. However, in order to establish the validity of the theory, the predictive power of these values of the contact angle and slip length should be demonstrated. This could have been done by Bach & Hassager if they had used these values of the contact angle and slip length to calculate the apparent contact angle at a half gap width of 0.060 cm, the experimentally reported value in Ngan & Dussan V. being 65°.

More definite conclusions can be drawn from the comparisons between theory and experiment if the dynamics of the fluid can accurately be described by the asymptotic limit correct to (including) $O(\mu U/\sigma)$ as $\mu U/\sigma \to 0$ holding L_s/a fixed, with $L_s/a \ll 1$. It will be shown in §2 that under these restricted conditions the dynamics of the fluids in the outer region depends on Θ and L_s only through the one parameter

$$\Theta + \frac{\mu U}{\sigma}\left\{\frac{2\sin\Theta}{\Theta - \cos\Theta\sin\Theta}\left[\ln\frac{a}{L_s} + 1\right] + l_i(\Theta)\right\}.$$

Here, the outer region refers to all the fluid excluding that residing instantaneously in the immediate vicinity of the moving contact line. The latter region is usually referred to as the inner region. The lengthscales of these two regions are denoted by a and L_s, respectively. The term $l_i(\Theta)$ depends directly on the form of the slip boundary condition, the parameter specified above being valid for other slip boundary conditions besides Navier's. Thus, under these restricted conditions, it is impossible to deduce unique values for Θ and L_s from measured characteristics of the flow field associated with the outer region, e.g. from the drag on any segment of the solid (even including a segment containing the moving contact line), or from a detailed description of the shape of the fluid interface. In fact, it is even impossible to deduce the appropriateness of Navier's slip boundary condition as opposed to those of others. On the other hand, this also implies the necessity of making only one comparison between theory and experiment at every contact line speed of interest in order to determine the value of this one parameter. Additional comparisons can then be viewed as providing tests by which the appropriateness of the slip boundary condition can be assessed. Thus, the very close agreement of the two comparisons between theory and experiment made by Bach & Hassager at the single contact line speed can be cited as evidence supporting the use of a slip boundary condition in fluid mechanics problems containing moving contact lines (provided, of course, that the conditions of the experiments of Ngan & Dussan V. correspond to the restricted conditions described above).

The objective of this study is to explore the extent to which the boundary-value problems defined in the outer region, correct to (including) $O(\mu U/\sigma)$ in the limit as $\mu U/\sigma \to 0$ holding L_s/a fixed for $L_s/a \ll 1$, describe the dynamics of a fluid body containing a moving contact line. In §2 the behaviour of the fluid within the matching region is examined since it provides boundary conditions for the dynamics of the fluid in the outer region. It is shown that the dynamics of the fluid within the

matching region depends upon the form of the slip boundary condition and the value of the contact angle through only one measurable parameter. It is also established that our objective can be achieved by comparing the experimentally measured shape of the fluid interface in the outer region as $r \to 0$ to its known form in the matching region. Since we are unable to make measurements of the shape of the fluid interface so close to the contact line, an indirect procedure for making this comparison is employed. This requires the formulation and solution of the boundary-value problem for the outer region associated with our experimental apparatus, refer to §§3 and 4, respectively. The experiments are presented in §5. In §6, the data and analysis are combined to deduce the shape of the fluid interface within the matching region. We end with a discussion of our results in §7.

2. Parameterization of the outer region

The objective of this section is to show that the effect of the moving contact line on the dynamics of the liquid in the outer region, correct to $O(\mu U/\sigma)$ in the limit as $\mu U/\sigma \to 0$, holding L_s/a fixed for $L_s/a \ll 1$, can be expressed in terms of one measurable material property of the system. The importance of this is clear: it enables predictions to be made about the dynamics of the fluids without knowing the physics of the fluids in the immediate vicinity of the moving contact line. Since determining the dynamics of the liquid correct to this order is not novel, we shall make free use of the already well-known asymptotic structure of the solution (refer to the work cited in §1.3 that use asymptotic methods, or, in the remainder of this section). Of the three dependent variables (interface shape, pressure field and velocity field) whose behaviour is sought in the outer region, it suffices to restrict our attention to the equations which describe the interface shape because they contain all the non-zero constants determined by matching (this includes the unknown pressure datum). Thus, we shall restrict our attention to examining the asymptotic structure near the moving contact line of only the solution for the interface shape. This section begins with an identification of these unknown constants and a review of their determination. We proceed by identifying the specific measurable material property referred to above, relating it to the parameter cited in §1, and using it to parameterize the solution in the outer region. The latter implies that measurements in the outer region cannot determine the individual values of the contact angle, the slip length, nor the details of the slip model. However, this does not preclude the ability to make predictions of the dynamics of the fluids on lengthscales large compared with the slip length.

The identification of the unknown constants and their determination can both be accomplished upon recalling the asymptotic forms of the solution for the interface shape in the inner and outer regions. It is convenient for these discussions to specify the shape of the interface in the form of the variation of its slope, θ, with distance from the contact line, r. Here, θ specifically denotes the angle formed between the local plane tangent to the fluid interface and the plane tangent to the solid wall. The asymptotic form of $\theta(r)$ in the matching region obtained from the solution valid in the inner region has been found to be:

$$\theta \sim \Theta + o(1) + \mu U/\sigma \left\{ \frac{2 \sin \Theta}{\Theta - \sin \Theta \cos \Theta} \left[\ln \frac{r}{L_s} + 1 \right] + l_i(\Theta) + o(1) \right\}, \tag{2.1}$$

valid as $r/L_s \to \infty$. The usual method of solution in the inner region involves an expansion of the boundary conditions at the fluid interface about the plane

intersecting the solid at the contact line at angle Θ. As examples: Hocking (1977) has calculated the value for $l_i(\Theta)$ (equivalent to $h_1/\sin\Theta$ in his notation) for the case of Navier's model (also refer to Hocking & Rivers 1982); Dussan V. (1976), her analysis restricted to the case $\Theta = \frac{1}{2}\pi$, found that $l_i(\frac{1}{2}\pi) \equiv 0$ for a family of slip models with wide-ranging characteristics. (As a consequence of her modelling assumption that any dependence of Θ on U should be expressed as a dependence of Θ on $\mu U/\sigma$, the additional term $\phi_{010}(0)$ appears. Our current approach regards $\Theta(U)$ as introducing a velocity scale which reflects the physics responsible for determining the value of the contact angle; consequently, the term $\phi_{010}(0)$ should be ignored.) On the other hand, the solution valid in the outer region gives:

$$\theta \sim \Theta_{00} + o(1) + \mu U/\sigma \left\{ \nu_0(L_s/a)\,[\Theta_{01} + o(1)] + \nu_1(L_s/a)\left[\frac{2\sin\Theta_{00}}{\Theta_{00} - \sin\Theta_{00}\cos\Theta_{00}} \left(\ln\frac{r}{a} + 1 \right) + l_0(\Theta_{00}) + c + o(1) \right] \right\}, \quad (2.2)$$

valid as $r/a \to 0$. Here, Θ_{00} denotes the slope of the interface correct to $O(1)$ as $\mu U/\sigma \to 0$, evaluated as $r/a \to 0$. (The interface at this order satisfies the same equation as that of a static interface shape, and is independent of L_s/a. It also represents the location in space about which the boundary conditions applied at the fluid interface for the outer problem are 'perturbed'.) Likewise, Θ_{01} denotes the slope of the $O(Ca)$ 'correction' to the interface shape, valid as $\mu U/\sigma \to 0$, and to lowest order as $L_s/a \to 0$, evaluated as $r/a \to 0$. The equation governing this mode is identical to that governing the 'corrections' to the interface shape under static conditions when the value of the contact angle has been perturbed by a small amount. Effects arising from the viscosity of the fluid in the outer region first appear in the ν_1 mode. The function $l_0(\Theta_{00})$ appearing in this mode shall be regarded as known, its explicit form depending on the dynamics and shape of the fluid in the outer region. The unknown constant c represents the pressure datum associated with the motion of the fluid at this order. Note that all of the unknown terms in the above two expressions for θ, consisting of Θ_{00}, $\nu_0\Theta_{01}$, ν_1, and c, occur in the outer solution, indicating in some sense that 'matching transfers information from the inner to the outer region'. Matching gives:

$$\Theta_{00} = \Theta, \quad \nu_0\Theta_{01} = \frac{2\sin\Theta}{\Theta - \sin\Theta\cos\Theta} \ln\frac{a}{L_s}, \quad \nu_1 = 1, \quad c = l_i - l_0.$$

Thus, knowledge of each term Θ, L_s, and l_i is required in order to determine the individual modes in the solution for θ valid in the outer region. An important additional consequence of matching not included in this presentation – correct to the orders of $\mu U/\sigma$ and L_s/a considered above – is the coincidence in the location of the contact line as perceived from both the inner and outer regions.

The material property of the system which shall be used to parameterize the dynamics of the liquid in the outer region is the slope of the interface, Θ_R, evaluated at a known small distance, R, from the moving contact line. It is essential that R lies within the matching region in order for Θ_R to be both in the outer region and a material property of the system (in the inner region). In order to identify a parameterization of the boundary-value problems arising in the outer region we begin by expressing (2.1) in terms of R and Θ_R, giving

$$\theta \sim \Theta_R + \mu U/\sigma \frac{2\sin\Theta_R}{\Theta_R - \sin\Theta_R\cos\Theta_R} \ln\frac{r}{R}, \quad (2.3)$$

where

$$\Theta_R \sim \Theta + \mu U/\sigma \left\{ \frac{2\sin\Theta}{\Theta - \sin\Theta\cos\Theta} \left[\ln\frac{R}{L_s} + 1 \right] + l_i(\Theta) \right\},$$

keeping in mind that these expressions are only valid to $O(\mu U/\sigma)$ as $\mu U/\sigma \to 0$. Note that this implies the parameter cited in §1 is equivalent to

$$\Theta_R + \mu U/\sigma \frac{2\sin\Theta_R}{\Theta_R - \sin\Theta_R\cos\Theta_R} \ln\frac{a}{R},$$

an expression entirely in terms of experimentally measurable quantities. Thus, an obvious parameterization of the boundary-value problems arising in the outer region is:

$$\theta_0 \sim \Theta_R \quad \text{as } r \to 0, \tag{2.4a}$$

$$\theta_1 \sim \frac{2\sin\Theta_R}{\Theta_R - \sin\Theta_R\cos\Theta_R} \ln\frac{r}{R} \quad \text{as } r \to 0, \tag{2.4b}$$

where $\theta \sim \theta_0 + \mu U/\sigma\, \theta_1 + \ldots$, (2.4*a*) and (2.4*b*) representing boundary conditions for the boundary-value problems arising in the outer region at $O(1)$ and $O(\mu U/\sigma)$, respectively.

Parameterizing the boundary-value problems in the outer region in terms of Θ_R is not novel. It was originally used by Hansen & Toong (1971); however, their implementation and justification were somewhat different. They correctly anticipated the lowest-order asymptotic form of the velocity field as $r/a \to 0$, i.e. as the location of the contact line is approached from the outer region, without any reference to modelling the physics governing the movement of the fluids in the immediate vicinity of the moving contact line. This approach was further pursued by Kafka & Dussan V. (1979). Their motivation was the same as that outlined above, although the details of their parameterization was slightly different.

3. Formulation

The objective of the analysis is to derive a relationship between the apex height, h, and the value of the intermediate contact angle, Θ_R, for the case of a viscous liquid displacing air between two parallel solid surfaces. As stated in §2, we need only analyse the dynamics of the fluid in the outer region. The system is viewed from a frame of reference at rest with respect to the moving contact line; thus, the two parallel solid surfaces, separated by a distance $2a$, appear to be moving at a constant speed, U, in the z-direction (the convention implies that the solid surfaces move downward in the $-z$-direction when $U > 0$). The origin of the coordinate system is located midway between the two plates and in the plane passing through the contact lines. The x- and z-axes point in the directions indicated in figure 1. The system is assumed to be at steady state in this frame of reference, with the dynamics of the fluid independent of the y-direction.

Scales are chosen to reflect the fact that we are interested in the case of a liquid displacing, or being displaced, by an immiscible fluid whose motion can be ignored. The *dimensional* position vector, velocity vector, and pressure field are denoted by (xa, za), (uU, wU), and $p\sigma/a$, respectively; σ denotes the surface tension. The pressure scale reflects the fact that we are focusing attention on situations in which the stresses due to surface tension dominate those due to viscosity.

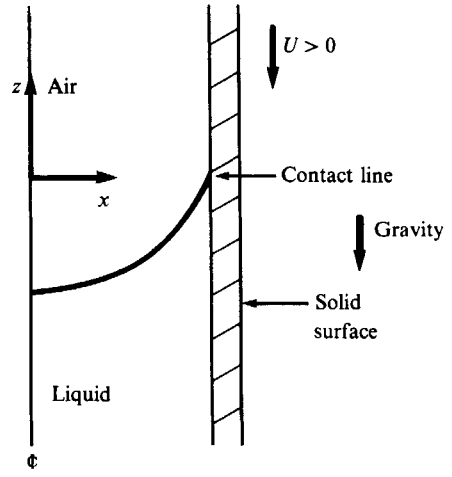

FIGURE 1. The configuration of half the system. The remainder is obtained by forming the mirror image about the ($x = 0$)-plane. The coordinate system (x, z) is in a frame of reference at rest with respect to the moving contact line.

The governing equations and boundary conditions are as follows. The dimensionless form of the Navier–Stokes and continuity equations are

$$Re\,Ca\{\boldsymbol{u}\cdot\nabla\boldsymbol{u}\} = -\nabla p + Ca\nabla^2\boldsymbol{u} - Bd\boldsymbol{k},$$

$$\nabla\cdot\boldsymbol{u} = 0,$$

where $\boldsymbol{u}$ denotes (u, w); Re denotes the Reynolds number, $Ua\rho/\mu$; Ca denotes the capillary number, $U\mu/\sigma$; Bd denotes the Bond number, $\rho g a^2/\sigma$. In these expressions, ρ and μ denote the density and viscosity of the liquid, respectively, and g denotes the gravitational constant, approximately equal to 980 cm/s^2. The group $Re\,Ca$ is often referred to as the Weber number. The kinematic and dynamic boundary conditions at the free surface are

$$\left.\begin{aligned}\boldsymbol{u}\cdot\boldsymbol{n} &= 0\\ \boldsymbol{T}\boldsymbol{n} &= \frac{\boldsymbol{n}}{R_{\mathrm{m}}}\end{aligned}\right\} \quad \text{at } z = f(x) \quad (-1 \leqslant x \leqslant 1),$$

where $\boldsymbol{n}$ denotes the unit outward normal from the liquid; $\boldsymbol{T}$ denotes the stress tensor; $(x, f(x))$ denotes the position of the free surface; R_{m} denotes the mean radius of curvature of the fluid interface

$$\frac{1}{R_{\mathrm{m}}} = \frac{\dfrac{\mathrm{d}^2 f}{\mathrm{d}x^2}}{\left\{1+\left(\dfrac{\mathrm{d}f}{\mathrm{d}x}\right)^2\right\}^{\frac{3}{2}}}.$$

The boundary conditions at the two parallel solid surfaces are

$$\boldsymbol{u} = -\boldsymbol{k} \quad \text{at } x = \pm 1, \quad z < 0,$$

where it is assumed that $U > 0$ for the liquid advancing over the solid, with the liquid located at positions $\{(x, z)\,|\,-1 \leqslant x \leqslant 1, -\infty < z \leqslant f(x)\}$. It is assumed that the far-field solution, i.e. the velocity and pressure fields as $z \to -\infty$, approaches two-

dimensional Poiseuille flow. Finally, as presented in §2, it is assumed that the slope of the interface has the following asymptotic structure as (x, z) approaches $(\pm 1, 0)$, the locations of the contact lines,

$$\theta \sim \Theta_R + Ca \frac{2 \sin \Theta_R}{\Theta_R - \sin \Theta_R \cos \Theta_R} \ln \frac{((1 \mp x)^2 + z^2)^{\frac{1}{2}}}{R/a},$$

where $\tan(\theta - \frac{1}{2}\pi) = \mathrm{d}f/\mathrm{d}x$. The fact that θ equals infinity at the contact line does not make this boundary condition unphysical because we are analysing the dynamics of the fluid in the outer region, i.e. the solution is not valid at (x, y) equals $(\pm 1, 0)$.

We seek a solution valid in the limit as *Bd*, *Ca*, and *Re* approach zero. It is assumed that the dependent variables can be represented as a regular asymptotic expansion of the form

$$V \sim V_0(x, z) + Bd\, V_{Bd}(x, z) + Ca\, V_{Ca}(x, z) + Re\, V_{Re}(x, z) + \ldots, \tag{3.1}$$

valid as *Bd*, *Ca*, and *Re* approach zero, where $\{V \mid \boldsymbol{u}, p, f\}$. A solution will be obtained to lowest order, V_0, for each of the dependent variables, and to first order in *Ca* and *Bd*, i.e. V_{Ca} and V_{Bd}, for both the pressure and the interface shape. Substituting the asymptotic expansions into the governing equations and boundary conditions generates a sequence of well-posed boundary-value problems.

3.1. *Lowest-order pressure field and interface shape*

The lowest-order pressure field and interface shape satisfy

$$\nabla p_0 = 0,$$

$$-p_0 = \frac{\dfrac{\mathrm{d}^2 f_0}{\mathrm{d}x^2}}{\left\{1 + \left(\dfrac{\mathrm{d}f_0}{\mathrm{d}x}\right)^2\right\}^{\frac{3}{2}}},$$

subject to the boundary conditions

$$f_0 = 0 \qquad \text{at } x = 1,$$

$$\frac{\mathrm{d}f_0}{\mathrm{d}x} = \cot \Theta_R \quad \text{at } x = 1,$$

$$\frac{\mathrm{d}f_0}{\mathrm{d}x} = 0 \qquad \text{at } x = 0,$$

where the last condition reflects the fact that the shape of the free surface is symmetrical about the $x = 0$ plane.

The solutions for p_0 and f_0 are

$$\begin{aligned} p_0 &= -\cos \Theta_R, \\ f_0 &= \tan \Theta_R - (\sec^2 \Theta_R - x^2)^{\frac{1}{2}}. \end{aligned} \tag{3.2}$$

Hence, the lowest-order pressure field is constant; the lowest-order interface shape is the arc of a circle.

3.2. *First-order in Bond number for the pressure field and interface shape*

The first-order pressure field and interface shape satisfy

$$\nabla p_{Bd} = -\boldsymbol{k},$$

$$\frac{\mathrm{d}}{\mathrm{d}x}\left\{\frac{\dfrac{\mathrm{d}f_{Bd}}{\mathrm{d}x}}{\left(1+\left(\dfrac{\mathrm{d}f_0}{\mathrm{d}x}\right)^2\right)^{\frac{3}{2}}}\right\} = -p_{Bd} \quad \text{at } z = f_0(x) \quad (-1 \leqslant x \leqslant 1),$$

subject to the boundary conditions

$$f_{Bd} = 0 \quad \text{at } x = 1,$$

$$\frac{\mathrm{d}f_{Bd}}{\mathrm{d}x} = 0 \quad \text{at } x = 1,$$

$$\frac{\mathrm{d}f_{Bd}}{\mathrm{d}x} = 0 \quad \text{at } x = 0.$$

The solutions are

$$p_{Bd} = -z + \tfrac{1}{2}\tan\Theta_R - \tfrac{1}{2}(\tfrac{1}{2}\pi - \Theta)\sec^2\Theta_R,$$

$$\frac{2f_{Bd}}{\sec^3\Theta} = \frac{\tan\Theta_R + (\tfrac{1}{2}\pi - \Theta_R)\sec^2\Theta_R - x\arcsin(x\cos\Theta_R)}{(\sec^2\Theta_R - x^2)^{\frac{1}{2}}} - 1 - (\tfrac{1}{2}\pi - \Theta_R)\tan\Theta_R. \tag{3.3}$$

3.3. *Lowest-order velocity field and first-order in capillary number for the pressure field and interface shape*

The lowest-order velocity field and leading order in capillary number for the pressure field satisfy:

$$0 = -\nabla p_{Ca} + \nabla^2 \boldsymbol{u}_0, \tag{3.4}$$

$$\nabla \cdot \boldsymbol{u}_0 = 0.$$

The continuity equation implies the existence of a stream function, ψ, with the property

$$\boldsymbol{u}_0 = (\partial\psi/\partial z, -\partial\psi/\partial x).$$

Substituting this representation of the velocity field into the curl of (3.4) gives:

$$\nabla^4\psi = 0. \tag{3.5}$$

The lowest-order form of the boundary conditions are: the kinematic boundary condition at the free surface

$$\psi = 0 \quad \text{at } z = f_0(x) \quad (-1 \leqslant x \leqslant 1); \tag{3.6}$$

the tangential component of the dynamic boundary condition at the free surface

$$T(\psi; \Theta_R) = 0 \quad \text{at } z = f_0(x) \quad (-1 \leqslant x \leqslant 1), \tag{3.7}$$

where

$$T((\cdot);\Theta_R) \equiv 2d_1\frac{\partial^2(\cdot)}{\partial x\,\partial z}+d_2\left[\frac{\partial^2(\cdot)}{\partial z^2}-\frac{\partial^2(\cdot)}{\partial x^2}\right],$$

$$d_1(x;\Theta_R) \equiv 2\frac{\mathrm{d}f_0/\mathrm{d}x}{1+(\mathrm{d}f_0/\mathrm{d}x)^2},$$

$$d_2(x;\Theta_R) \equiv \frac{(\mathrm{d}f_0/\mathrm{d}x)^2-1}{1+(\mathrm{d}f_0/\mathrm{d}x)^2};$$

the normal component of the dynamic boundary condition at the free surface

$$\frac{\mathrm{d}}{\mathrm{d}x}\frac{\mathrm{d}f_{Ca}/\mathrm{d}x}{\{1+\mathrm{d}f_0/\mathrm{d}x^2\}^{\frac{1}{2}}} = -p_{Ca}+N(\psi;\Theta_R) \quad \text{at } z=f_0(x) \quad (-1\leqslant x\leqslant 1), \tag{3.8}$$

where

$$N((\cdot);\Theta_R) \equiv 2d_2\frac{\partial^2(\cdot)}{\partial x\,\partial z}-d_1\left[\frac{\partial^2(\cdot)}{\partial z^2}-\frac{\partial^2(\cdot)}{\partial x^2}\right];$$

the boundary conditions at the contact line

$$f_{Ca}=0 \quad \text{at } x=1, \tag{3.9}$$

$$\frac{\mathrm{d}f_{Ca}}{\mathrm{d}x} \sim \frac{2}{(\Theta_R-\sin\Theta_R\cos\Theta_R)\sin\Theta_R}\ln\left(\frac{((1-x)^2+z^2)^{\frac{1}{2}}}{R/a}\right) \quad \text{as } (x,z)\to(1,0), \tag{3.10}$$

$$\frac{\mathrm{d}f_{Ca}}{\mathrm{d}x}=0 \quad \text{at } x=0; \tag{3.11}$$

the boundary conditions at the two parallel solid surfaces

$$\psi=0 \quad \text{at } x=\pm 1, \quad z\leqslant 0; \tag{3.12}$$

$$\frac{\partial\psi}{\partial x}=1 \quad \text{at } x=\pm 1, \quad z\leqslant 0; \tag{3.13}$$

and the stream function far from the free surface

$$\psi\to\tfrac{1}{2}(x^3-x) \quad \text{as } z\to-\infty. \tag{3.14}$$

The solutions for ψ, p_{Ca}, and f_{Ca} are presented in §4.

4. Solutions for ψ, p_{Ca} and f_{Ca}

The boundary-value problem defined by (3.5)–(3.7), (3.9), (3.10) and (3.11) can be solved, at least in part, using a technique introduced by Smith (1952). Smith obtained a representation of the solution to the following boundary-value problem in the form of an eigenfunction expansion:

$$\nabla^4\chi=0 \quad \text{for } \{(x,z)\,|-1\leqslant x\leqslant 1,-\infty<z\leqslant 0\}, \tag{4.1}$$

$$\chi=\frac{\partial\chi}{\partial x}=0 \quad \text{at } x=\pm 1, \quad -\infty<z\leqslant 0, \tag{4.2}$$

$$\left.\begin{aligned}\frac{\partial^2\chi}{\partial z^2}&=b_1(x)\\ \frac{\partial^2\chi}{\partial x^2}&=b_2(x)\end{aligned}\right\} \quad \text{at } z=0, \quad -1\leqslant x\leqslant 1, \tag{4.3a, b}$$

$$\chi\to 0 \quad \text{as } z\to-\infty, \quad -1\leqslant x\leqslant 1, \tag{4.4}$$

where both $b_1(x)$ and $b_2(x)$ are considered to be known functions satisfying the constraints

$$\int_{-1}^{+1} b_1(x)\,dx = 0, \tag{4.5}$$

$$\int_{-1}^{+1} b_2(x)\,x\,dx = 0. \tag{4.6}$$

This differs from our problem in a number of significant ways. The domains of the two problems are not the same. Smith's problem is defined on the domain $\{(x,z)\,|\,-1 \leqslant x \leqslant 1, z \leqslant 0\}$, its boundaries being composed of constant coordinate curves. In contrast, part of the boundary of the domain of our problem, $\{(x,z)\,|\,-1 \leqslant x \leqslant 1, z = f_0(x)\}$, is not a constant coordinate curve. Hence, part of our method of solution consists of determining the specific forms of $b_1(x)$ and $b_2(x)$ on $z = 0$ so that ψ satisfies (3.6) and (3.7) along $\{(x,z)\,|\,-1 \leqslant x \leqslant 1, z = f_0(x)\}$. (Once the solution for ψ has been obtained, its value within the region containing no liquid, $\{(x,z)\,|\,-1 \leqslant x \leqslant 1, f_0(x) < z \leqslant 0\}$, is ignored.) There are other significant differences between the two problems. Unlike Smith's problem, all of the following functions are inhomogeneous; $\partial\psi/\partial x$ at $x = \pm 1$, ψ as $z \to -\infty$, and $\partial\psi/\partial x$† as $x \to \pm 1$ at $z = 0$, which necessitates expressing ψ as the superposition of three parts. Also, in our problem ψ does not converge uniformly as $x \to \pm 1$ and $z \to 0$. Thus, our method for determining $b_1(x)$ and $b_2(x)$ utilizes knowledge of their asymptotic forms as $x \to \pm 1$, which minimizes the inconveniences that would naturally arise from the non-uniform convergence of the eigenfunction expansion of ψ.

4.1. *Superposition of ψ, and solution of ψ_A*

The stream function ψ is represented as the sum of three parts

$$\psi = \tfrac{1}{2}(x^3 - x) + \psi_A + \psi_B, \tag{4.7}$$

where ψ_A satisfies

$$\nabla^4 \psi_A = 0 \quad \text{for } \{(x,z)\,|\,-1 \leqslant x \leqslant 1,\ -\infty < z \leqslant 0\}, \tag{4.8}$$

$$\psi_A = \frac{\partial \psi_A}{\partial x} = 0 \quad \text{at } x = \pm 1,\ -\infty < z \leqslant 0, \tag{4.9}$$

$$\left.\begin{aligned} &\frac{\partial^2 \psi_A}{\partial z^2} = 0 \\ &\psi_A = \frac{(x^3 - x)\,(\frac{1}{2}\pi \tan \Theta_R - 1)\sin 2\Theta_R}{2(\sin 2\Theta_R - 2\Theta_R)} \end{aligned}\right\} \quad \text{at } z = 0, \quad -1 \leqslant x \leqslant 1, \tag{4.10a, b}$$

$$\psi_A \to 0 \quad \text{as } z \to -\infty, \quad -1 \leqslant x \leqslant 1. \tag{4.11}$$

The solution for ψ_A can readily be obtained using the Fourier sine transformation in the z-direction. It is given by

$$\psi_A = \frac{2}{\pi}\frac{(\frac{1}{2}\pi \tan \Theta_R - 1)\sin 2\Theta_R}{(\sin 2\Theta_R - 2\Theta_R)} \int_{-\infty}^{0} \frac{1}{\tau}\left\{\frac{(1-x)\sinh(1+x)\tau}{2\tau - \sinh 2\tau} - \frac{(1+x)\sinh(1-x)\tau}{2\tau - \sinh 2\tau} - \tfrac{1}{2}(x^3 - x)\right\} \sin z\tau\,d\tau. \tag{4.12}$$

† To show that Smith's problem is characterized by $\partial\psi/\partial x = 0$ at $x = \pm 1$ and $z = 0$, integrate (4.6) by parts. This gives $\partial\psi/\partial x|_{x=1} = \psi(1,0)$. The term on the right-hand side of the equation is zero as a consequence of (4.2), and ψ being continuous over the entire domain. Asymmetry of ψ in x has been used.

Hence, the function ψ_B must satisfy

$$\nabla^4\psi_B = 0 \quad \text{for } \{(x,z)\,|-1 \leqslant x \leqslant 1, \quad -\infty \leqslant z \leqslant 0\}, \tag{4.13}$$

$$\psi_B = \frac{\partial\psi_B}{\partial x} = 0 \quad \text{at } x = \pm 1, \quad -\infty < z \leqslant 0, \tag{4.14}$$

$$\left.\begin{aligned} \psi_B &= -\tfrac{1}{2}(x^3 - x) - \psi_A \\ T(\psi_B;\Theta_R) &= -3xd_2 - T(\psi_A;\Theta_R) \end{aligned}\right\} \quad \text{at } z = f_0(x), \quad -1 \leqslant x \leqslant 1, \tag{4.15a, b}$$

$$\psi_B \to 0 \quad \text{as } z \to -\infty, \quad -1 \leqslant x \leqslant 1, \tag{4.16}$$

where the expressions on the right-hand side of (4.15*a*, *b*) are considered to be known in light of (4.12). The determinations of the variations of ψ_A and the second partial derivatives of ψ_A with respect to x and z evaluated along $z = f_0(x)$ arising in the expression $T(\psi_A;\Theta_R)$ and $N(\psi_A;\Theta_R)$, refer to (3.8), are accomplished by numerically integrating the inverse Fourier-sine transformation after interchanging the orders of differentiation and integration. Gauss–Laguerre quadrature (15 points) is used in the integrations over the semi-infinite domain $(-\infty, 0]$. In each case, the asymptotic forms for the integrands, in the limit as the integration variable goes to infinity, are subtracted from the integrands and only the differences are numerically integrated. The integrals of the asymptotic forms can be expressed in closed form. Approximate solutions for ψ_B are obtained in the next subsection using Smith's method, suitably modified.

Before proceeding, an explanation is in order for the boundary conditions given by (4.10 *a*, *b*). As already mentioned, $\partial\psi/\partial x \to 0$ as $x \to \pm 1$ at $z = 0$ in Smith's problem. However, a local analysis of the velocity field in the neighbourhood of $(x,z) = (\pm 1, 0)$ reveals that in our problem $\partial\psi/\partial x \to 1 + (\frac{1}{2}\pi \tan\Theta_R - 1)\sin 2\Theta_R/(\sin 2\Theta_R - 2\Theta_R)$, refer to the Appendix. Hence, Smith's eigenfunction expansion cannot be used to represent $\psi - \frac{1}{2}(x^3 - x)$. However, it can be used to represent $\psi - \frac{1}{2}(x^3 - x) - \psi_A$; where ψ_A satisfies (4.8), (4.9), (4.11), and with the following replacing (4.10*a*, *b*)

$$\left.\begin{aligned} \frac{\partial^2\psi_A}{\partial z^2} &= g_1(x) \\ \psi_A &= g_2(x) \end{aligned}\right\} \quad \textit{at } z = 0, \quad -1 \leqslant x \leqslant 1,$$

where $g_1(x)$ and $g_2(x)$ denote any given set of asymmetric functions, provided $\mathrm{d}g_2/\mathrm{d}x$ approaches a non-zero value as $x \to \pm 1$. Choosing $g_1 \equiv 0$ and $g_2 \equiv \frac{1}{2}(x^3 - x)(\frac{1}{2}\pi \tan\Theta_R - 1)\sin 2\Theta_R/(\sin 2\Theta_R - 2\Theta_R)$ simplifies the determination of ψ_B.

4.2. *Solution for ψ_B and ψ*

Our method has at its heart Smith's eigenfunction expansion representation of the solution to (4.1)–(4.4). A solution of the following form is sought

$$\begin{bmatrix} \partial^2\chi/\partial z^2 \\ \partial^2\chi/\partial x^2 \end{bmatrix} = \sum_n c_n \mathrm{e}^{s_n z} \begin{bmatrix} \phi_1(x;s_n) \\ \phi_2(x;s_n) \end{bmatrix}, \tag{4.17}$$

where each eigenfunction

$$\begin{bmatrix} \phi_1 \\ \phi_2 \end{bmatrix}$$

and eigenvalue s_n satisfies

$$\begin{bmatrix} \mathrm{d}^2/\mathrm{d}x^2 & 0 \\ 0 & \mathrm{d}^2/\mathrm{d}x^2 \end{bmatrix} \begin{bmatrix} \phi_1 \\ \phi_2 \end{bmatrix} = -s_n^2 \begin{bmatrix} 0 & -1 \\ 1 & 2 \end{bmatrix} \begin{bmatrix} \phi_1 \\ \phi_2 \end{bmatrix}, \tag{4.18}$$

$$\phi_1 = \frac{\mathrm{d}\phi_1}{\mathrm{d}x} = 0 \quad \text{at } x = \pm 1, \quad z < 0. \tag{4.19}$$

Explicit forms for χ are obtained by integrating twice either scalar equation given by (4.17). For example, integrating twice the first equation in (4.17) with respect to z, and using (4.4) gives

$$\chi = \sum_n \frac{c_n}{s_n^2} \mathrm{e}^{s_n z} \phi_1(x; s_n). \tag{4.20}$$

The solutions to (4.18) and (4.19) consist of both even and odd functions of x. We need only the odd functions

$$\phi_1(x; s_n) = \tfrac{1}{2} s_n \{(1-x)\sin(1+x)\, s_n - (1+x)\sin(1-x)\, s_n\},$$

$$\phi_2(x; s_n) = -\phi_1 + \cos(1-x)\, s_n - \cos(1+x)\, s_n,$$

for $\sin 2s_n = 2s_n$, excluding $s_0 \equiv 0$. If $\{s_n\}$ denotes the eigenvalues located in the positive orthant, then the complete set of eigenvalues consists of

$$\{s_n\} \cup \{\bar{s}_n\} \cup \{-s_n\} \cup \{-\bar{s}_n\}.$$

The eigenvalues $\{s_n\}$ are determined to machine precision by a standard Newton–Raphson procedure. Initial guesses are obtained from their asymptotic form as $n \to \infty$

$$2s_n \sim (2n + \tfrac{1}{2})\pi + \mathrm{i} \ln(4n+1)\pi.$$

Convergence is extremely fast, no more than three iterations are required. The boundary condition denoted by (4.4) implies that

$$\begin{bmatrix} \partial^2\chi/\partial z^2 \\ \partial^2\chi/\partial x^2 \end{bmatrix} = 2\,\mathrm{Re}\left\{ \sum_{n=1}^{\infty} c_n \mathrm{e}^{s_n z} \begin{bmatrix} \phi_1 \\ \phi_2 \end{bmatrix} \right\}, \tag{4.21}$$

where Re denotes the real part of a complex function. The constants $\{c_n\}$ can be regarded as the expansion coefficients of b_1 and b_2 in terms of the eigenfunctions

$$\begin{bmatrix} \phi_1 \\ \phi_2 \end{bmatrix},$$

as can be seen by setting $z = 0$ in (4.21) and making use of (4.3a, b), giving

$$\begin{bmatrix} b_1 \\ b_2 \end{bmatrix} = 2\,\mathrm{Re}\left\{ \sum_{n=1}^{\infty} c_n \begin{bmatrix} \phi_1 \\ \phi_2 \end{bmatrix} \right\}. \tag{4.22}$$

The constants $\{c_n\}$ are determined by taking the inner product of

$$\begin{bmatrix} b_1 \\ b_2 \end{bmatrix}$$

with the eigenfunctions of the adjoint problem $[\phi_1^* \phi_2^*]$, giving

$$\bar{c}_n = \frac{1}{k_n} \int_{-1}^{+1} [\phi_1^*(x; s_n)\, \phi_2^*(x; s_n)] \begin{bmatrix} 0 & -1 \\ 1 & 2 \end{bmatrix} \begin{bmatrix} b_1 \\ b_2 \end{bmatrix} \mathrm{d}x, \tag{4.23}$$

where

$$[\phi_1^* \phi_2^*]\begin{bmatrix} \mathrm{d}^2/\mathrm{d}x^2 & 0 \\ 0 & \mathrm{d}^2/\mathrm{d}x^2 \end{bmatrix} = -s_n^2[\phi_1^* \phi_2^*]\begin{bmatrix} 0 & -1 \\ 1 & 2 \end{bmatrix}, \tag{4.24}$$

$$\phi_1^* = \frac{\mathrm{d}\phi_1^*}{\mathrm{d}x} = 0 \quad \text{at } x = \pm 1, \tag{4.25}$$

and

$$k_n \equiv \int_{-1}^{+1} [\phi_1^*(x; s_n)\, \phi_2^*(x; s_n)]\begin{bmatrix} 0 & -1 \\ 1 & 2 \end{bmatrix}\begin{bmatrix} \phi_1(x; s_n) \\ \phi_2(x; s_n) \end{bmatrix} \mathrm{d}x. \tag{4.26}$$

The solution to (4.24) and (4.25) is

$$\left.\begin{aligned} \phi_1^*(x; s_n) &= \phi_1(x; s_n) + \cos(1-x)\, s_n - \cos(1+x)\, s_n, \\ \phi_2^*(x; s_n) &= \phi_1(x; s_n), \end{aligned}\right\} \tag{4.27a, b}$$

with the same set of eigenvalues as before. Substituting the above into (4.26) gives

$$k_n = -4 \sin^4 s_n. \tag{4.28}$$

This completes the solution to Smith's problem. Discussions of existence, convergence, and completeness can be found in Joseph (1977), Joseph & Sturges (1975, 1978), Gregory (1980*a*, *b*) and Joseph, Sturges & Warner (1982).

The function χ identified above represents the solution for ψ_B in our problem, provided (4.15*a*, *b*) are satisfied. This is accomplished by using the appropriate functions for $b_1(x)$ and $b_2(x)$. In order to determine the values of b_1 and b_2, we begin by assuming that they can be expressed as follows

$$\begin{bmatrix} b_1 \\ b_2 \end{bmatrix} = 2\,\mathrm{Re}\left\{\sum_{n=1}^{\infty} e_n \begin{bmatrix} \phi_1 \\ \phi_2 \end{bmatrix}\right\} + \begin{bmatrix} \dfrac{4x \sin 2\Theta_R}{(\sin 2\Theta_R - 2\Theta_R)(1-x^2)} \\ 0 \end{bmatrix}. \tag{4.29}$$

The second term on the right-hand side of (4.29) is chosen so that the series containing the unknown constants $\{e_n\}$ converges uniformly as $x \to \pm 1$, refer to the Appendix. It follows from (4.22), (4.23), (4.27*a*, *b*) and (4.28) that

$$\begin{bmatrix} \dfrac{4x \sin 2\Theta_R}{(\sin 2\Theta_R - 2\Theta_R)(1-x^2)} \\ 0 \end{bmatrix} = -2\,\mathrm{Re}\left\{\sum_{n=1}^{\infty} \frac{[1 - \cos 2s_n - s_n Si(s_n)] \sin 2\Theta_R}{(\sin 2\Theta_R - 2\Theta_R) \sin^4 s_n} \begin{bmatrix} \phi_1 \\ \phi_2 \end{bmatrix}\right\}, \tag{4.30}$$

where *Si* denotes the sine integral (Abramowitz & Stegun 1964). The expansion of ψ_B follows directly from (4.20) and (4.30) and is given by

$$\psi_B = 2\,\mathrm{Re}\left(\sum_{n=1}^{\infty}\left[e_n - \frac{[1 - \cos 2s_n - s_n Si(s_n)] \sin 2\Theta_R}{(\sin 2\Theta_R - 2\Theta_R) \sin^4 s_n}\right] \frac{\mathrm{e}^{s_n z}}{s_n^2} \phi_1(x; s_n)\right\} \tag{4.31}$$

The relationships which $\{e_n\}$ must satisfy are generated by substituting (4.31) into (4.15*a*, *b*)

$$\begin{aligned} 2\,\mathrm{Re}\left\{\sum_{n=1}^{\infty} e_n \mathrm{e}^{s_n f_0(x)} \begin{bmatrix} \phi_1/s_n^2 \\ D_T \end{bmatrix}\right\} &= \begin{bmatrix} -\frac{1}{2}(x^3 - x) - \psi_A \\ -3x d_2 - T(\psi_A; \Theta_R) \end{bmatrix} \\ &+ 2\,\mathrm{Re}\left\{\sum_{n=1}^{\infty} \frac{[1 - \cos 2s_n - s_n Si(s_n)] \sin 2\Theta_R\, \mathrm{e}^{s_n f_0(x)}}{(\sin 2\Theta_R - 2\Theta_R) \sin^4 s_n} \begin{bmatrix} \phi_1/s_n^2 \\ D_T \end{bmatrix}\right\}, \end{aligned} \tag{4.32}$$

where $D_T \equiv (2d_1/s_n)\,\mathrm{d}\phi_1/dx + d_2(-\phi_2+\phi_1)$. All the terms on the right-hand side of (4.32) are known functions of x.

The set of unknown constants $\{e_n\}$ are determined in the following manner. The series on the left-hand side of (4.32) is terminated at $n = N$, for varying values of N between 1 and 10. A set of N linearly independent equations are obtained by requiring the remainder of the series to be orthogonal to the set of vectors

$$\left\{\begin{bmatrix}\phi_1/s_n^2\\ D_T\end{bmatrix} \mid n = 1,\ldots,N\right\}.$$

The *ad hoc* assumption is made that the constants $\{e_n^N \mid n = 1,\ldots,N\}$ are real.† The superscript has been included to distinguish between the different approximate solutions. The resulting set of equations are

$$\sum_{i=1}^{N} M_{ij}\, e_i^N = d_j \quad \text{for } j = 1,\ldots,N, \tag{4.33}$$

where

$$M_{ij} \equiv 4\int_{-1}^{+1}\left[\mathrm{Re}\left\{\frac{\mathrm{e}^{s_i f_0(x)}\phi_1}{s_i^2}\right\}\mathrm{Re}\left\{\frac{\mathrm{e}^{s_j f_0(x)}\phi_1}{s_j^2}\right\} + \mathrm{Re}\{\mathrm{e}^{s_i f_0(x)} D_T\}\,\mathrm{Re}\{\mathrm{e}^{s_j f_0(x)} D_T\}\right]\mathrm{d}x,$$

and

$$d_j \equiv -2\int_{-1}^{+1}\left[\{\tfrac{1}{2}(x^3-x)+\psi_A\}\,\mathrm{Re}\left\{\frac{\mathrm{e}^{s_j f_0(x)}}{s_j^2}\right\} + \{3xd_2 + T(\psi_A;\Theta_R)\}\,\mathrm{Re}\{\mathrm{e}^{s_j f_0(x)} D_T\}\right]\mathrm{d}x$$

$$+4\int_{-1}^{+1}\sum_{n=1}^{\infty}\left[\mathrm{Re}\left\{\frac{[1-\cos 2s_n - s_n Si(s_n)]\sin 2\Theta_R\, \mathrm{e}^{s_n f_0(x)}\phi_1}{s_n^2(\sin 2\Theta_R - 2\Theta_R)\sin^4 s_n}\right\}\mathrm{Re}\left\{\frac{\mathrm{e}^{s_j f_0(x)}\phi_1}{s_j^2}\right\}\right.$$

$$\left.+\,\mathrm{Re}\left\{\frac{[1-\cos 2s_n - s_n Si(s_n)]\sin 2\Theta_R\, \mathrm{e}^{s_n f_0(x)} D_T}{(\sin 2\Theta_R - 2\Theta_R)\sin^4 s_n}\right\}\mathrm{Re}\{\mathrm{e}^{s_j f_0(x)} D_T\}\right]\mathrm{d}x.$$

The most inconvenient aspect of the problem is the slow convergence of the infinite series appearing in the expression for $\{d_j\}$ as $x \to \pm 1$, resulting from the decreasing influence of the negative exponential as $f_0(x)$ approaches zero. Gauss–Legendre quadrature is used to numerically integrate the terms in $\{M_{ij}\}$ and $\{d_j\}$. The first hundred values of $\{1-\cos 2s_n - s_n Si(s_n)\}$ are determined by a straight-line integration between eigenvalues using the 20-point Gauss–Legendre quadrature routine modified for complex variables. The remaining terms are obtained by evaluating the asymptotic form of the sine-integral. For each series appearing in

† This assumption was not made intentionally. It arose as a consequence of the scheme we followed to identify the best set of trail functions to expand

$$\begin{bmatrix}b_1\\ b_2\end{bmatrix} - \begin{bmatrix}\dfrac{4x\sin 2\Theta_R}{(\sin 2\Theta_R - 2\Theta_R)(1-x^2)}\\ 0\end{bmatrix}.$$

All of our calculations were completed when we realized the lack of necessity, also the lack of desirability, of this assumption.

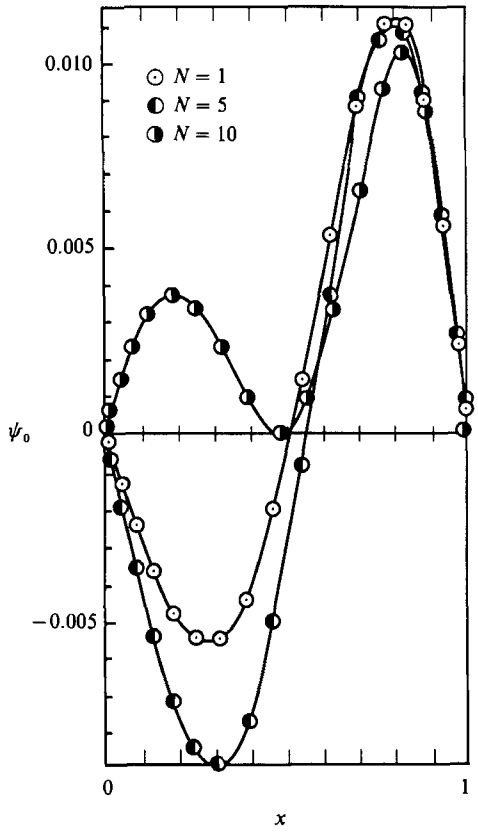

FIGURE 2. The lowest-order stream function $\psi_0(x, z; \Theta_R, N)$ on $z = f_0(x)$ for $\Theta_R = 30°$ and $\{N | 1, 5, 10\}$.

(4.33), the asymptotic forms of the n term is subtracted from the n term, and only these differences are summed numerically; closed form expressions are obtained for the summations of the asymptotic forms. This accelerates the convergence of the part of the series summed numerically. Note that a good solution in the neighbourhood of the contact line is needed because the contact-angle boundary condition is imposed on the interface in this region. The matrix inversion routine used to solve (4.33) is a double precision algorithm that utilizes Gauss–Jordan elimination with the maximum pivot strategy (White 1983).

As already stated, (4.33) has been solved for N varying from 1 to 10. Figures 2 and 3 give the evaluation of (3.6) and (3.7) for $0 \leqslant x < 1$, respectively, at $\Theta_R = 30°$, that is, $\psi = 0$, and $T(\psi; 30°) = 0$ at $z = f_0(x)$ for $0 \leqslant x < 1$. We choose this value of Θ_R for illustrative purposes because it is typical of the values used to analyse our experimental results. It is evident from these figures that even the solution corresponding to the case when N equals 10 has an error. The improvement in satisfying (3.7) is evident as N varies in value from 1 to 10,† but there is only a small improvement in satisfying (3.6). We feel that the most likely cause is the *ad hoc*

† Although there appears to be a large error in satisfying (3.7) as $x \to 1$, the relative error is actually small. This is a consequence of the rapidly increasing value of the components of the stress tensor as $x \to 1$.

assumption discussed above that $\{e_n^N \mid n = 1, \ldots, N\}$ are real. The complete solution for the stream function is

$$\psi = \frac{1}{\pi}\int_{-\infty}^{0} \frac{2(\frac{1}{2}\pi\tan\Theta_R - 1)\sin 2\Theta_R}{\tau(\sin 2\Theta_R - 2\Theta_R)}\left[\frac{(1-x)\sinh(1+x)\tau}{2\tau-\sinh 2\tau} - \frac{(1+x)\sinh(1-x)}{2\tau-\sinh 2\tau} - \tfrac{1}{2}(x^3-x)\right]\sin z\tau\,\mathrm{d}\tau + \tfrac{1}{2}(x^3-x) + 2\,\mathrm{Re}\left\{\sum_{n=1}^{N}\frac{e_n^N\,\mathrm{e}^{s_n z}\phi_1}{s_n^2} - \sum_{n=1}^{\infty}\frac{[1-\cos 2s_n\,Si(s_n)]\sin 2\Theta_R}{s_n^2[\sin 2\Theta_R - 2\Theta_R]\sin^4 s_n}\mathrm{e}^{s_n z}\phi_1\right\} \tag{4.34}$$

4.3. *Solution for* p_{Ca}

The first-order pressure field is obtained by substituting (4.34), the solution for ψ, into (3.4) and integrating. This gives

$$p_{Ca} = c_p - 3z\left[1+(-1+\tfrac{1}{2}\pi\tan\Theta_R)\frac{\sin 2\Theta_R}{\sin 2\Theta_R - 2\Theta_R}\right] - \frac{4}{\pi}(-1+\tfrac{1}{2}\pi\tan\Theta_R)\frac{\sin 2\Theta_R}{\sin 2\Theta_R - 2\Theta_R} \times \int_{-\infty}^{0}\left[\frac{\sinh(1+x)\tau+\sinh(1-x)\tau}{2\tau-\sinh 2\tau}\right]\cos\tau z\,\mathrm{d}\tau - 2\,\mathrm{Re}\left\{\sum_{n=1}^{N} e_n^N\,\mathrm{e}^{s_n z}[\sin(1-x)s_n + \sin(1+x)s_n] + \sum_{n=1}^{\infty}\frac{[1-\cos 2s_n - s_n\,Si(s_n)]\sin 2\Theta_R}{[\sin 2\Theta_R - 2\Theta_R]\sin^4 s_n}\mathrm{e}^{s_n z}[\sin(1-x)s_n + \sin(1+x)s_n]\right\}, \tag{4.35}$$

where c_p denotes the pressure datum which is evaluated when solving for f_{Ca}, the first order interface shape.

4.4. *Solution for* f_{Ca}

The first-order interface shape is determined by (3.8). A more explicit form of this equation is obtained by evaluating $N(\psi; \Theta_R)$ using the solution for ψ given by (4.34); thus

$$\frac{\mathrm{d}}{\mathrm{d}x}\frac{\mathrm{d}f_{Ca}/\mathrm{d}x}{(1+(\mathrm{d}f_0/\mathrm{d}x)^2)^{\frac{3}{2}}} = -p_{Ca} + 3d_1 x + \frac{3(-1+\frac{1}{2}\pi\tan\Theta_R)\sin 2\Theta_R}{\sin 2\Theta_R - 2\Theta_R} \times\left(d_1 x + \frac{4d_2}{3\pi}\int_{-\infty}^{0}\frac{\mathrm{d}\Lambda}{\mathrm{d}x}\cos\tau z\,\mathrm{d}\tau + \frac{4d_1}{3\pi}\int_{-\infty}^{0}\{\tau\Lambda + E\}\sin\tau z\,\mathrm{d}\tau\right) + 2\,\mathrm{Re}\left\{\sum_{n=1}^{\infty}\frac{[1-\cos 2s_n - s_n\,Si(s_n)]\sin 2\Theta_R}{[\sin 2\Theta_R - 2\Theta_R]\sin^4 s_n}\mathrm{e}^{s_n f_0(x)}D_N + \sum_{n=1}^{N} e_n^N\,\mathrm{e}^{s_n f_0(x)}D_N\right\} \tag{4.36}$$

where

$$E \equiv \frac{-\cosh(1+x)\tau + \cosh(1-x)\tau}{2\tau-\sinh 2\tau},$$

$$\Lambda \equiv \frac{(1-x)\sinh(1+x)\tau - (1+x)\sinh(1-x)\tau}{2\tau-\sinh 2\tau},$$

$$D_N \equiv \frac{2d_2}{s_n}\frac{\mathrm{d}\phi_1}{\mathrm{d}x} - d_1(\phi_1-\phi_2).$$

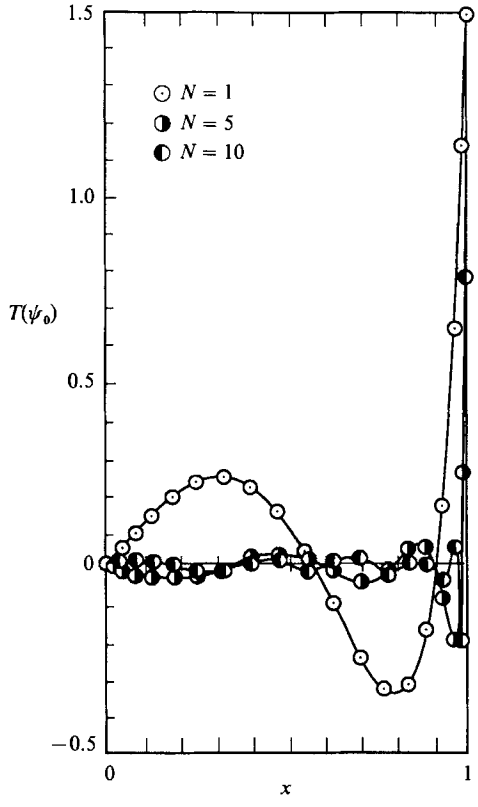

FIGURE 3. The tangent stress due to the lowest-order solution $T[\psi_0(x, z; \Theta_R, N); \Theta_R]$ on $z = f_0(x)$ for $\Theta_R = 30°$ and $\{N | 1, 5, 10\}$.

R/a...	0.005	0.007	0.01	0.015	0.02
Θ_R					
20°	58.0	52.1	46.0	39.2	34.5
25°	35.1	31.5	27.8	23.7	20.9
30°	23.2	20.9	18.4	15.7	13.8
35°	16.4	14.8	13.0	11.1	9.81
40°	12.2	10.9	9.67	8.27	7.30
45°	9.36	8.43	7.46	6.39	5.66
50°	7.44	6.71	5.94	5.10	4.52
55°	6.06	5.47	4.86	4.18	3.71
60°	5.05	4.57	4.06	3.50	3.12
R/a...	0.03	0.05	0.07	0.1	0.15
Θ_R					
20°	28.3	21.0	16.7	12.6	8.77
25°	17.0	12.6	10.0	7.58	5.26
30°	11.3	8.44	6.68	4.67	3.22
35°	8.04	5.99	4.78	3.65	2.58
40°	6.00	4.50	3.60	2.77	1.98
45°	4.66	3.51	2.83	2.19	1.59
50°	3.74	2.83	2.29	1.79	1.31
55°	3.08	2.34	1.91	1.49	1.10
60°	2.59	1.98	1.62	1.27	0.942

TABLE 1. Evaluation of $f_{Ca}(0; \Theta_R, R/a)$. R/a and Θ_R must satisfy $(R/a)\sin\Theta_R > 0.005$.

The solution of f_{Ca} is obtained by integrating (4.36) twice, subject to the boundary conditions expressed by (3.9), (3.10) and (3.11). Since the infinite series appearing on the right-hand side of (4.36) and in the expression for p_{Ca} does not converge uniformly as $x \to \pm 1$, that is, near the contact line, special care must be taken when performing the two integrations. Techniques similar to those discussed in the subsection pertaining to the solution of ψ_B concerning the evaluation of $\{d_j\}$ are used. The inverse Fourier sine and cosine transformations are evaluated using the technique discussed in the subsection containing the solution of ψ_A. Integration of the well-behaved terms on the right-hand side of (4.36) are obtained using a single precision version of the cubic spline routines available from the IMSL library. Refer to Ngan (1985) for details.

Our primary results consist of the contribution by f_{Ca} to the apex height, that is, the evaluation of $f_{Ca}(0; R/a, \Theta_R)$ for a range of values of both R/a and Θ_R, refer to table 1. The entries in table 1 are based upon only one trial function, i.e. $N = 1$; including more terms did not sufficiently increase the accuracy of the solution to justify the additional computer time. This indicates that a substantial portion of the solution for the shape of the interface comes from ψ_A and the asymptotic form of ψ_B as (x, z) approaches the location of the contact line. That is to say, the error associated with only approximately satisfying (3.6) and (3.7) may have only a marginal effect on the value of $f_{Ca}(0; R/a, \Theta_R)$.

5. Experiments

5.1. *Description of experiments*

As in our previous study (Ngan & Dussan V. 1982), 1000 centistroke Union Carbide L-45 silicone oil was used to displace air in a vertical parallel-plate geometry; refer to figure 4. Silicone oil was chosen because its surface tension is relatively insensitive to most surface active agents; hence, contamination is a lesser concern. Cells were constructed of two glass microscope slides (Corning 2947 plain lot no. 100583A) separated by one or more stainless steel spacers (shim stock or plate of 0.01, 0.0275, 0.07 or 0.12 cm nominal thickness) forming separations, $2a$, of 0.01, 0.02, 0.0275, 0.0375, 0.055, 0.08 and 0.12 cm. Thus, seven separations were investigated in this study whereas only three were investigated in the previous study. The side and bottom edges of the slides were sealed with PTFE tape, and 0.25 in. thick Plexiglas plates were used to distribute the load over the surface. The silicone oil was introduced into the bottom of the cell through a short length (approximately 8 in.) of Teflon tubing (Cole–Parmer R-6417-31 having 0.032 in. i.d. and 0.064 in. o.d.) by a Sage Model 355 variable speed positive-displacement syringe pump. We did not observe the oscillations reported earlier when using the Harvard syringe pump. The experiments were performed at 25.0 ± 0.5 °C. The density and surface tension of the silicone oil are respectively 0.97 g cm^{-3} and 19.7 dyn cm^{-1}.

The method of pretreating the slides was adapted from one used to prepare slides for the vapour deposition of metals. Instead of pretreating slides singly, how sets of slides were treated so that the entire set would be exposed to the same conditions. Eight sets of slides were placed through the following procedure. From a box containing 72 slides, 30 slides are selected at random, and placed, at random, into a polypropylene slide staining rack (Kartell 380 from Markson JD5952). The rack is then immersed in 500 ml of rapidly boiling distilled, deionized water, brought to a second boil, and then boiled for 10 more minutes. The slides are submerged into four additional baths, and then dried in an oven at 60 °C. The premise is that any

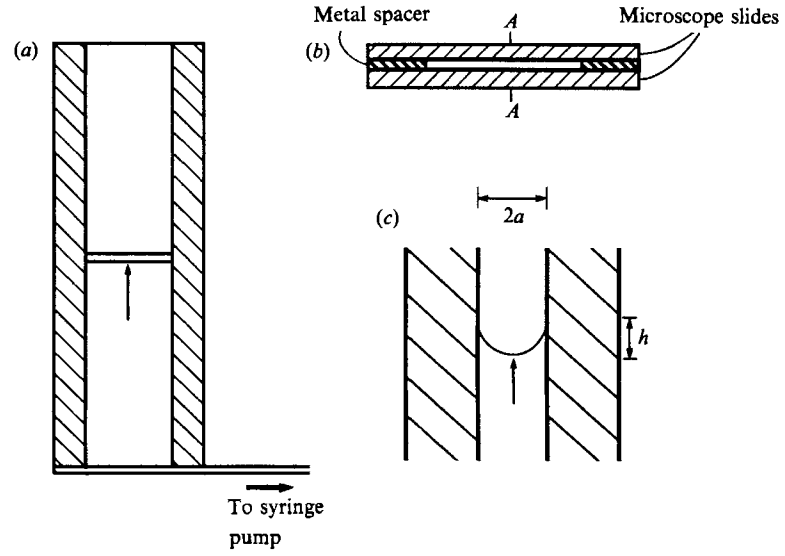

FIGURE 4. Depiction of a cell. It is composed of two microscope slides separated by stainless steel spacers. Three perspectives are shown: (*a*) elevation (1:1), ratio of illustration to actual size; (*b*) plan (2:1); and (*c*) section *A*–*A* of (*b*) (12:1). The arrows in (*a*) and (*c*) indicate the direction of motion of the silicone oil.

material on the surface of the glass will partition itself between the surface phase and the bulk liquid, or in the case of surface active contaminants, be removed by the rising bubbles and carried to the surface of the liquid. After drying, the slides are removed from the staining racks and placed into a random slot in one of three microscope slide storage boxes, ten to a box (five in each half).

In the construction of a cell, one slide from each half of one of the boxes was selected at random; the next two cells were constructed from slides from the other two boxes. Hence, a total of 240 slides were pretreated and stored, 80 to a box (capacity 100), permitting the construction of up to 120 cells. At least 15 cells could be constructed for each size slot, with another 15 remaining to be used in case of leakage, breakage, measurement or calibration complications, and mistakes. The two staining racks were boiled in distilled, deionized water prior to their first contact with the slides. This precaution was taken in order to remove free monomer, plasticizer, or other extractable additives that might have been present in the polypropylene.

The slot thickness was determined by locating the inside surfaces of the slides along the edges of the cell under a microscope and measuring the separation using a calibrated reticle. The value of the slot thickness used in the calculations for any one cell represents the average of ten measurements, five from each edge of the cell. An independent test indicates that these measurements at the edges give values comparable to those obtained from measurements near the middle of the cell.

The movement of the interface was observed through and recorded by an optical system as depicted in figure 5. A wide-angle zoom lens (Vivitar Series I 24–48 mm) was used in the reverse position to obtain a better image. A 35 mm camera (Nikon FM) was equipped with a motor drive unit (Nikon MD-11) so that images could be obtained at rates of almost four frames per second. All components except the cell holder were mounted on an optical rail atop a granite table; the cell holder was placed onto a translating stage also mounted to the table. This permitted the use of a fixed camera-to-lens distance because focusing could be accomplished by moving

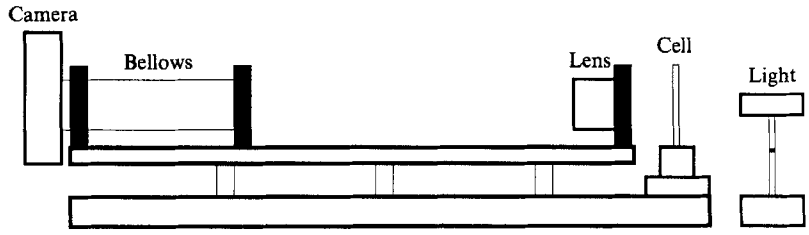

FIGURE 5. The optical system used for observing and recording the images of the interface as it advances up the vertical slot.

the cell. Hence, for all cells, a fixed magnification of 33.75 × was obtained by using a focal length of 24 mm, at an extension of 810 mm. The images were recorded on a fine-grain black-and-white panchromatic film (Kodak Technical Pan Film 2415) and developed in a diluted high energy developer (Kodak HC-110, dilution D) for lower grain and higher resolution. An exposure index of 125 is expected if the film is developed for 8 min at 20 °C. At these conditions, the contract index is 1.75 and the gamma is 2.00 (see Kodak pamphlet no. P-255 for more details.) It was found that slightly darker negatives were needed; hence, the film was developed for the equivalent of 10 min at 20°. Optical distortion, checked by photographing a stage micrometer, was found to be negligible over the field of view. The stage micrometer was also used to provide the lengthscale for determining the actual magnification from the photographs.

When backlit, and observed from the perspective depicted in figure 4(*a*), the interfaces appeared as dark bands on a bright field. These bands were horizontal in the field of view, indicating that edge effects due to the spacers were negligible, and that the plates were parallel. For the air ⟷ silicone oil ⟷ glass system, the top side of a band is one of the contact lines, while the bottom side is the apex of the meniscus; hence, an apex height h can readily be determined by measuring the thickness of the band.

The other quantity obtained from the photographic images was the velocity of the contact line. Velocities were calculated from the change in position of the contact line in successive frames, knowing the time interval between frames. The speed of the motor drive was calibrated every eighth roll (after each set of the seven different slot sizes). Linear interpolation was used to determine the speed for each run. The experiments were designed to be conducted at constant velocity; uncertainty in the selection of the syringe pump setting and leakage were the major obstacles that had to be overcome.

In all, sixty-three cells were assembled; however, data were unobtainable from six of these runs due to severe leakage (3), poor contrast in the photographic negatives (2), and an incorrect syringe pump setting (1). Of the fifty-seven remaining cells, eleven each were of the 0.01 and 0.02 cm slotwidths, and seven each were of the other sizes. The larger number of runs were performed in the smaller slots because it is more difficult to obtain data at any pre-chosen contact line speed. These cells are prone to leakage and breakage due to the higher pressures developed in narrower slots. In addition, small leaks represent a larger fraction of the delivered flow, and hence, give rise to data at velocities much lower than anticipated. Note that, since data obtained from slots of different sizes are to be compared at the same velocity, leakage gives rise to data that are essentially unusable.

A contact line speed of about 0.030 cm s^{-1}, corresponding to a capillary number of

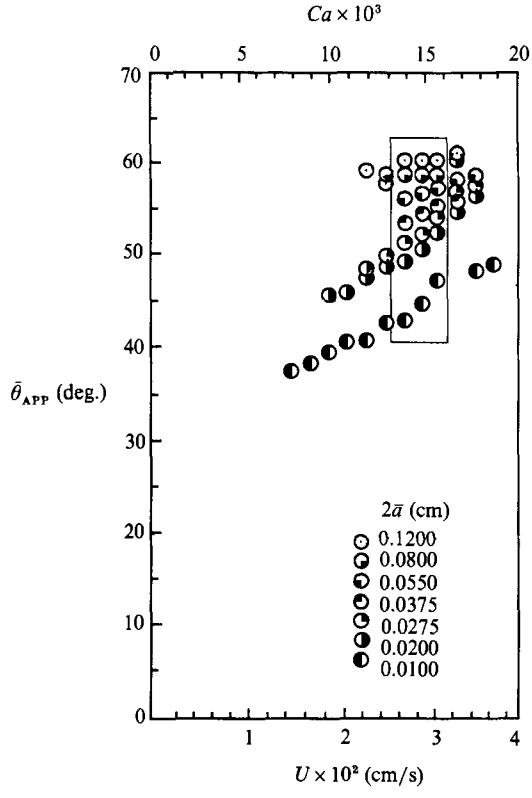

FIGURE 6. The variation of the apparent contact angles calculated from the mean dimensionless apex heights with the contact line speeds, U, and the corresponding value of Ca indicated along the abscissa for the seven slot widths listed in the legend.

about 0.015, was chosen as the point of comparison. A smaller Ca would have been preferred, but previous experiments with a nearly identical material system had indicated that there might be insufficient dependence of the apparent contact angle on the size of the slot at that speed to ensure a sufficient separation of the curves. The data from the narrower slots also seemed to be more reliable there than at lower speeds. Finally, data were obtained that span a range of capillary numbers, a consequence of leakage, uncertainties in the determination of the contact line locations and frame-to-frame time intervals, and slight variations in the slotwidths of cells meant to be the same size.

5.2. *Experimental data*

The data are presented in figure 6. Mean values of the slotwidth and dimensionless apex height, $\overline{2a}$ and $\overline{h/a}$, and their sample standard deviations were calculated for each of the seven sizes of slots and for each capillary number interval of width 0.001. The mean dimensionless apex heights were converted into mean apparent contact angles using:

$$\Theta_{APP} = \cos^{-1}\frac{-2\overline{h/a}}{1+\overline{h/a}^2}. \tag{5.1}$$

Represented in the figure are 1427 points from a total of 1549; samples with less than ten points are not presented.

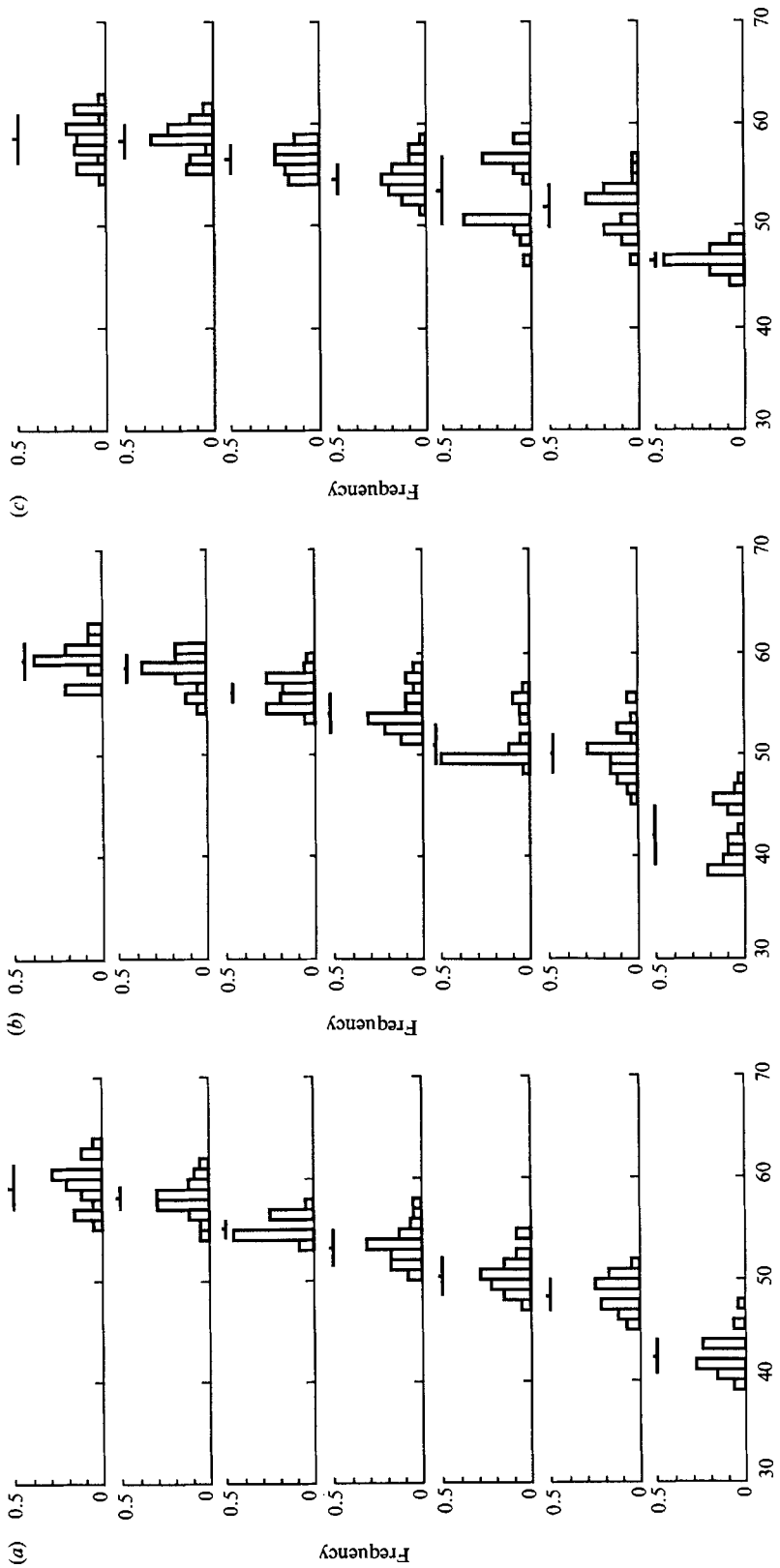

FIGURE 7. Conditional distributions of the apparent contact angle for Ca within the three different ranges: (*a*) $0.013 < Ca < 0.014$, (*b*) $0.014 < Ca < 0.015$, (*c*) $0.015 < Ca < 0.016$. Above each histogram is a vertical dash that denotes the value of the apparent contact angle corresponding to $\overline{h/a}$ and a horizontal line that denotes the range of the angles enclosed by $\overline{h/a} \pm \delta_H$.

$0.013 < Ca < 0.014$					$0.014 < Ca < 0.015$				
Θ^-_{APP}	$\bar{\Theta}_{APP}$	Θ^+_{APP}	$\bar{a}$	N_E	Θ^-_{APP}	$\bar{\Theta}_{APP}$	Θ^+_{APP}	$\bar{a}$	N_E
40.32	42.27	44.25	0.00525	37	40.82	43.92	47.10	0.00525	28
46.87	48.64	50.44	0.01035	43	47.65	49.92	52.22	0.01035	39
48.50	50.60	52.72	0.01405	26	48.56	51.36	54.21	0.01405	31
51.51	53.15	54.81	0.01915	35	52.13	53.98	55.85	0.01910	40
54.30	55.30	56.31	0.02775	28	54.66	56.08	57.51	0.02770	40
56.71	58.18	59.66	0.04120	27	56.60	58.21	59.83	0.04120	46
57.18	59.30	61.45	0.06170	19	57.51	59.47	61.46	0.06170	35

$0.015 < Ca < 0.016$				
Θ^-_{APP}	$\bar{\Theta}_{APP}$	Θ^+_{APP}	$\bar{a}$	N_E
45.51	46.43	47.36	0.00545	14
49.43	51.69	53.97	0.01040	32
49.80	53.21	56.68	0.01385	22
53.07	54.69	56.32	0.01905	54
55.20	56.45	57.70	0.02785	54
56.71	58.39	60.09	0.04120	58
57.30	59.44	61.61	0.06145	71

TABLE 2. Data pertaining to the conditional distributions of figures 7, 8 and 9. N_E represents the number of data points within the particular histogram. $\bar{a}$ is the average half slotwidth in cm. Θ^-_{APP}, $\bar{\Theta}_{APP}$ and Θ^+_{APP} are the three apparent contact angles in degrees corresponding to the dimensionless apex heights $\overline{h/a}+s_H$, $\overline{h/a}$ and $\overline{h/a}-s_H$, respectively.

It should be emphasized that this figure represents the dynamic behaviour of the apparent contact angle for one particular material system: air$\longleftrightarrow$1000 cstk L-45 silicone oil$\longleftrightarrow$Corning 2947 glass slides. Therefore, the apparent angles are plotted as a function of the contact line speed. A capillary number scale is also indicated because it is the pertinent dimensionless group that appears in the theoretical analysis.

The 779 data points falling into the three intervals of Ca ranging between 0.013 and 0.016, enclosed by the box in figure 6, are presented as histograms in figure 7. It is only within these three intervals that there are a sufficient number of points to calculate mean apparent angles for all seven slot sizes. In each histogram, the relative frequency is plotted for values of the apparent contact angle in one degree increments, for each type of slot. Above each histogram is a vertical dash that denotes the location of the apparent contact angle corresponding to $\overline{h/a}$ and a horizontal line that denotes the range of angles enclosed by $\overline{h/a}\pm s_H$, s_H denoting a sample standard deviation of $\overline{h/a}$. The number of points included in each histogram, the average slotwidth, and the angles mentioned are listed in table 2.

6. Determination of (R, Θ_R)

An essential step of establishing self-consistency between the theory and experiments consists of determining the extent to which (2.3) is satisfied. Since Θ_R represents the slope of the interface at any radial distance R from the contact line within the matching region, the combination (R, Θ_R) appearing in (2.3) is not unique but rather forms a continuous one-parameter family of values denoted by $\{(R, \Theta_R)\}$. The members of this family are (r, θ), where θ satisfies (2.3) and r takes on any value within the matching region. Direct experimental measurement of the radial

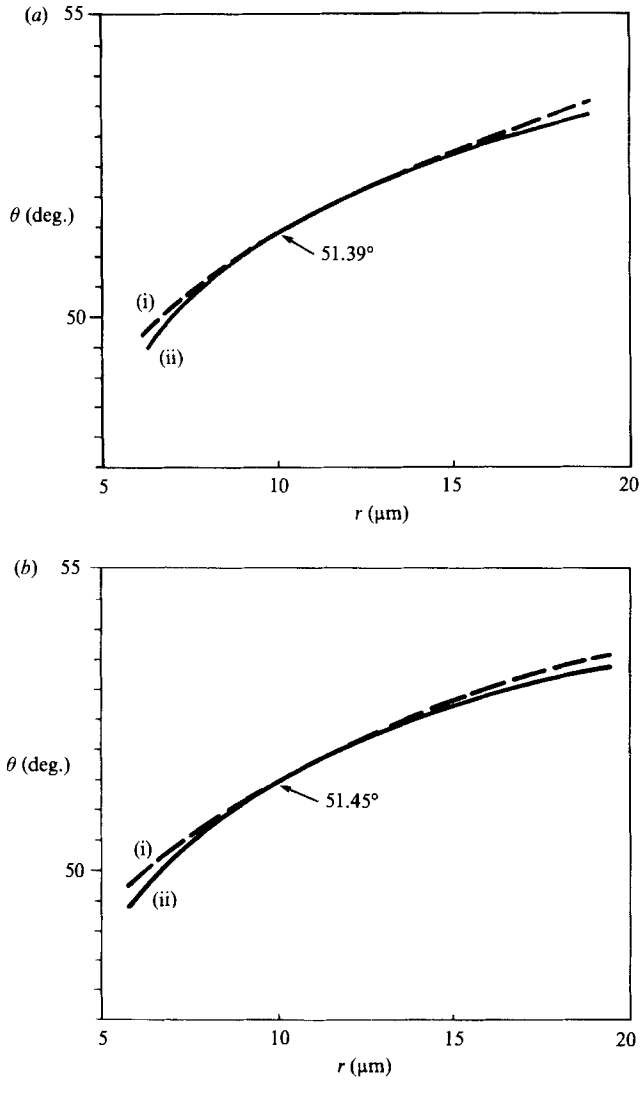

FIGURE 8. For caption see facing page.

dependence of the slope of the interface in the immediate vicinity of the moving contact line would be ideal. Since this was not done we can only infer the slope of the interface within the matching region using the measured apex height in conjunction with our theoretical calculations. We begin by presenting the method adopted to make this inference. In part, this requires identifying a specific range of r to be regarded as the matching region. The section concludes with comparisons between the inferred slope of the interface near the moving contact line and (2.3). Demonstrations of the extent to which the theory and the deduced family $\{(R, \Theta_R)\}$ predict the individual experimental measurements are also presented.

An element in the family $\{(R, \Theta_R)\}$ is identified by fixing the value of R, and then determining the value of Θ_R which minimizes S, where

$$S \equiv \frac{1}{M} \sum_{i=1}^{M} \left\{ f\left(0; \frac{R}{a_i}, \Theta_R, Ca, Bd\right) - \left(\frac{\bar{h}}{a}\right)_i \right\}^2. \tag{6.1}$$

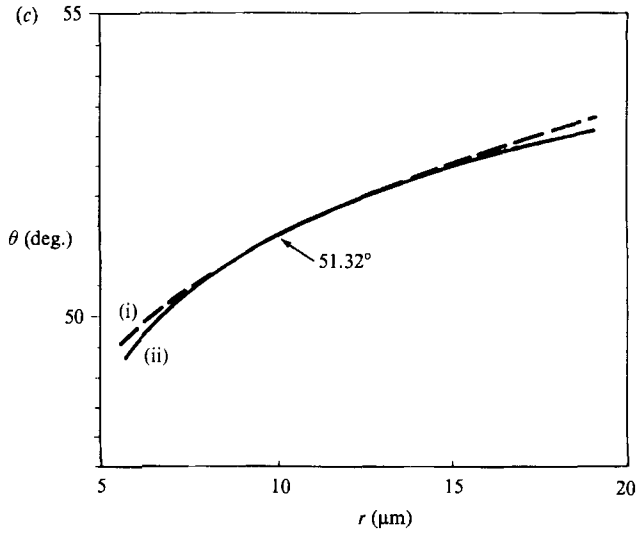

FIGURE 8. The family $\{(R, \Theta_R)\}$ for Ca within the three different ranges: (*a*) $0.013 < Ca < 0.014$, (*b*) $0.014 < Ca < 0.015$, (*c*) $0.015 < Ca < 0.016$. Curve (i) is determined by minimizing S using experimental data associated with the four largest gap widths. Curve (ii) coincides with curve (i) at R equals 10 μm, while satisfying (2.3).

Here, $(\overline{h/a})_i$ denotes the average experimentally measured (apex height/half gap width) at a particular gap width $\overline{a_i}$ corresponding to one of the three intervals of Ca indicated in table 2. The values of $(\overline{h/a})_i$ are obtained from the tabulated values of $\bar{\Theta}_{\mathrm{APP}}$ using (5.1). The term M denotes the total number of gap widths being considered. The expression for the theoretically predicted (apex height/half gap width), f, results from substituting (3.2) and (3.3), both evaluated at $x = 0$, into (3.1), giving

$$f \sim \tan\Theta_R - \sec\Theta_R + \rho g \overline{a_i}^2/\sigma \frac{\{\sin\Theta_R - 1\}\{1 - (\frac{1}{2}\pi - \Theta_R)\sec\Theta_R\}}{2\sin^3\Theta_R} + U\mu/\sigma f_{Ca}(0; R/\overline{a_i}, \Theta_R), \tag{6.2}$$

where f_{Ca} is evaluated by interpolating between entries in table 1. The entire family $\{(R, \Theta_R)\}$ is obtained by determining the value of Θ_R that minimizes S for every value of R within the matching region.

The matching region and M must both be identified before $\{(R, \Theta_R)\}$ can be determined. Strictly speaking, matching does not take place within a specific region; rather, it has meaning only in a limiting sense. Nevertheless, we shall regard the matching region as the range of r within which the shape of the interface obeys (2.3) to the degree of accuracy inherent in our calculations. The portion of the matching region accessible by our calculations shall be denoted by $\mathscr{R}$. We have chosen $\mathscr{R} \equiv \{r \mid 0.01 < r/a < 0.1\}$. The lower bound is a consequence of the limitations of the accuracy of the calculations presented in §4. It represents the smallest value of R/a appearing in table 1 that can be used consistent with the values of Θ_R of interest. The upper bound represents the approximate value of r beyond which the geometry of the outer region has a noticeable effect on the interface shape. One direct consequence of these limits is the restriction imposed on the maximum value of M. Since $\{R/\overline{a_i} \mid i = 1, \ldots, M\}$ must be in $\mathscr{R}$, the only values of $\mathscr{R}$ which can be used in the

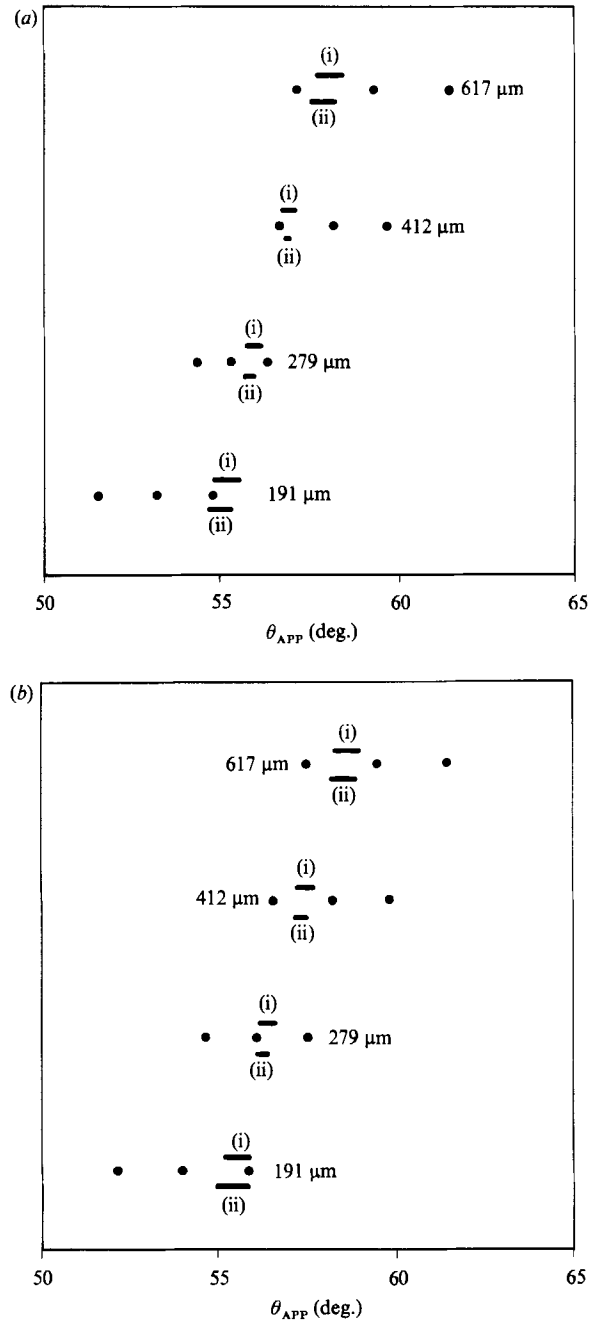

FIGURE 9(a+b). For caption see facing page.

determination of $\{(R, \Theta_R)\}$ by the method described above lie within the interval $(0.01\overline{a_1} < R < 0.1\overline{a_M})$. This assumes the elements of the set $\{\overline{a_i}\}$ are ordered as follows $\overline{a_1} > \overline{a_2} \ldots > \overline{a_M}$. In order for this interval to retain a reasonable size we have chosen $M = 4$. For example, when $\{\overline{a_i} \mid i = 1, \ldots, 4\}$ denote the four largest gap widths then $\{R \mid 6 \times 10^{-4} < R < 19 \times 10^{-4}$ cm$\}$.

At a given value of Ca, the analysis is most accurate within regions where the

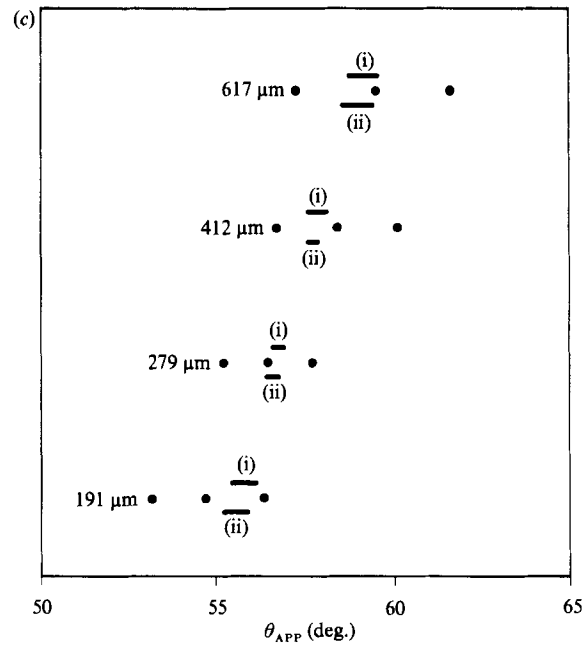

FIGURE 9. Theoretically predicted values for the apparent contact angles for the four largest gap widths, and for Ca within the three different ranges: (*a*) $0.013 < Ca < 0.014$, (*b*) $0.014 < Ca < 0.015$, (*c*) $0.015 < Ca < 0.016$. The lines (i) and (ii) correspond to the predictions based on the $\{(R, \Theta_R)\}$ of curves (i) and (ii) in figure 8, respectively. The values of Θ^-_{APP}, $\bar{\Theta}_{APP}$ and Θ^+_{APP} are indicated by ● at each gap width.

interface experiences the least amount of viscous bending. Viscous bending decreases with increasing distance away from the moving contact line. Hence, the greater the value of the lower bound of R, the smaller the amount of viscous bending to the interface between R and the apex, and the greater the accuracy of table 1. Thus, the four largest gap widths have been used to determine the family $\{(R, \Theta_R)\}$. Curves (i) in figure 8 give the results of the calculations. The three separate evaluations in the figure correspond to the three intervals of Ca used to group the experimental data. The ability of $\{(R, \Theta_R)\}$ to predict the experimentally measured apex heights at the four gap widths is illustrated in figure 9. The length of the lines labelled (i) indicate the range of values of Θ_{APP} obtained using the evaluations in table 1 at the entire family $\{(R, \Theta_R)\}$ in (6.2) and (5.1).

There are various features of these figures worth noting. Although each member of $\{(R, \Theta_R)\}$ was obtained through a separate minimization calculation, the entire family predicts the same value of Θ_{APP} to within $\pm 0.5°$ at each gap width. This is a necessary characteristic in order for $\{(R, \Theta_R)\}$ to describe the shape of the interface within the matching region. The fact that $\{(R, \Theta_R)\}$ agrees well with (2.3) is illustrated by curves (ii) in figure 8, where (R, Θ_R) appearing in (2.3) is set equal to (10^{-3} cm, 51.39°), a member of $\{(R, \Theta_R)\}$. All of these features indicate agreement between theory and experiment. However, it is evident from figure 9 that a systematic deviation exists between theoretical predictions and experimental measurements of Θ_{APP} at the four different gap widths. It remains unclear whether this lack of agreement should be attributed to systematic errors in the experiments, inaccuracies in the theoretical calculations, or, the inappropriateness of the approach presented in §2 for analysing moving contact line problems.

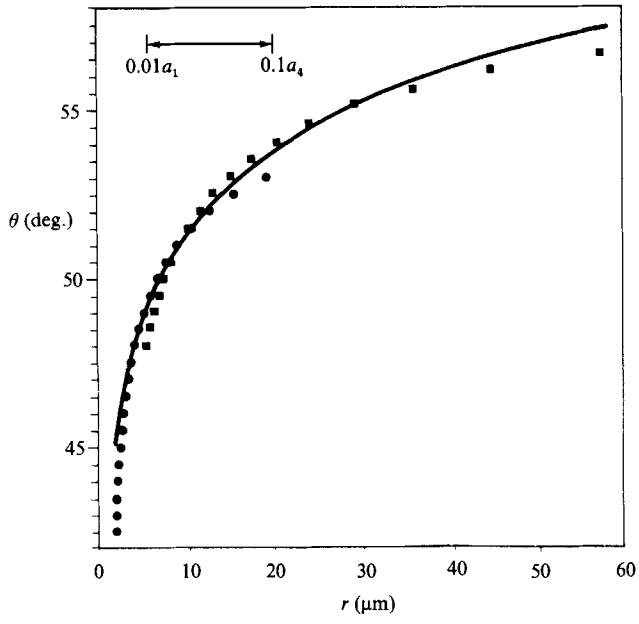

FIGURE 10. The variation of the slope of the interface generated by table 1 for ●, $a = 191$ μm; ■, $a = 617$ μm, and ——, (2.3), all assuming $(R, \Theta_R) = (10$ μm, 51.39°).

We conclude with some comparisons among different theoretical evaluations of the interface shape which serves to illustrate the extent of some of the errors present in our calculations. Regardless of the appropriateness of the approach presented in §2 to describe the experiments, all of the points on curves (ii) in figure 8 should predict (using table 1, (5.1), and (6.2)) the same value of Θ_{APP} at each gap width. Instead, a range of values are predicted as indicated by each line (ii) in figure 9. This could be a consequence of computational inaccuracies, or of locating the range of R too far from the moving contact line. It is of interest to note that the length of lines (i) in figure 9 obtained using the experimental data, are no longer than (ii). The degree to which $\mathscr{R}$ represents the matching region can be further illustrated by comparing the shape of the interface given by (2.3) setting (R, Θ_R) equal to $(10^{-3}$ cm, 51.39°), with that generated by table 1 for the largest and the smallest of the four gap widths; refer to figure 10. Our solutions begin deviating from (2.3) at approximately dimensionless r equal to 0.07, somewhat less than the value of 0.1 assumed above.

7. Discussion

The objective of this study has been to determine the appropriate boundary-value problem which describes the dynamics of the fluid excluding that lying instantaneously in the immediate vicinity of the moving contact line. We chose to investigate the validity of the boundary-value problem defined in the outer region generated by using a slip boundary condition on the surface of the solid. In §2 it was shown that the boundary condition originating from the matching region can be expressed in a form containing *one* measurable parameter, refer to (2.3). (It is worth noting that there may be a plethora of mechanisms describing the behaviour of the fluid in the immediate vicinity of the moving contact line consistent with (2.3) besides slip boundary conditions. Thus, establishing the validity of (2.3), in and of

itself, does not imply that the fluid slips along the surface of the solid.) Thus, the boundary-value problem in the outer region can be re-expressed in a form containing no explicit reference to a slip boundary condition. Thus, the heart of our investigation has focused on establishing the extent to which (2.3) accurately describes the shape of the fluid interface near the moving contact line in the outer region asymptotically as $r \to 0$, and for small values of Ca.

The validity of (2.3) was investigated using an indirect technique. It is based upon our derived relationship (6.2) between the slope of the interface within the matching region, Θ_R, evaluated at a radial distance, R, from the moving contact line and the apex height of the meniscus, h, the quantity measured in our experiments. Our technique for determining Θ_R was presented in §6. It consists of identifying the value of Θ_R which minimizes the deviation between theoretically predicted and experimentally measured values of h/a over a range of gap widths. The dependence of the slope of the fluid interface on the radial distance from the contact line is obtained by repeating this calculation for a range of values of R corresponding to the matching region. The results of these calculations are denoted by the family $\{(R, \Theta_R)\}$.

Comparisons between theory and experiment appear in §6. They consist of: (i) determining the extent to which $\{(R, \Theta_R)\}$ satisfies (2.3), where the terms (r, θ) and (R, Θ_R) appearing in (2.3) denote any two members of the family $\{(R, \Theta_R)\}$, and, (ii) calculating the values of h/a using any member of $\{(R, \Theta_R)\}$ and all the different gap widths, and comparing these values to the experimental measurements. Our principal results are contained in figures 8 and 9. As discussed in §6, we feel that they indicate agreement between theory and experiment, although falling somewhat short of being definitive. Figure 8 illustrates rather close agreement between (2.3) (curve ii), and the slope of the interface determined by our indirect method (curve i). The fact that every point on curve (i) in figure 8 predicts the same value of Θ_{APP} (an alternative representation of h/a, refer to (5.1)) at each gap width (more precisely, the prediction is to within $\pm 0.5°$ of the same value of Θ_{APP}), is illustrated by curve (i) in figure 9. On the other hand, it is evident from the three comparisons in figure 9, corresponding to the different contact line speeds, that the theory consistently predicts a weaker dependence of Θ_{APP} on the gap width that that measured experimentally. Even if we restrict our attention to the case giving the best agreement between theory and experiment, that corresponding to a Ca of 0.0155, one still finds a systematic, as opposed to a random, deviation between the predictions and the measurements.

The cause of the systematic deviation between the theory and the experiments is at this point unclear. The most obvious potential source arises from the fact that the theory accounts for only the two lowest orders in an asymptotic expansion in Ca valid in the limit as $Ca \to 0$. A value of Ca of the order of 10^{-2} may be too large to be accurately covered by such a theory. It is interesting to note that at these values of Ca our calculations indicate that the $O(Ca)$ mode is already contributing about 10% of the slope in the matching region.

Appendix

The variable r is made dimensionless with a in the Appendix. The asymptotic form of the stream function valid in the limit as $z \to 0$ and $x \to 1$ corresponding to the lowest-order velocity field will be identified. The most straightforward approach makes use of the local polar coordinate system (r, ϕ) given by the following relationships:

$1-x = r\sin\phi; z = -r\cos\phi$. In this coordinate system the boundary conditions are: $\partial^2\psi/\partial\phi^2 = 0$ and $\psi = 0$ on $\phi = \Theta_R$ for $r > 0$; and, $r^{-1}\partial\psi/\partial\phi = -1$ and $\psi = 0$ on $\phi = 0$ for $r > 0$. It is easily shown that a solution for ψ is given by

$$\psi \sim \{\sin\phi - \phi[\tan\Theta_R \sin\phi + \cos\phi]\}\frac{r\sin 2\Theta_R}{\sin 2\Theta_R - 2\Theta_R} - r\sin\phi,$$

or, equivalently by

$$\psi \sim \left\{1-x+[(1-x)\tan\Theta_R - z]\arctan\frac{(1-x)}{z}\right\}\frac{\sin 2\Theta_R}{\sin 2\Theta_R - 2\Theta_R} - 1 + x. \qquad \text{(A 1)}$$

It is readily established that

$$\frac{\partial\psi}{\partial x} \sim 1 + \frac{(\frac{1}{2}\pi\tan\Theta_R - 1)\sin 2\Theta_R}{\sin 2\Theta_R - 2\Theta_R} \quad \text{on } z = 0^-.$$

Since the above is not zero, Smith's technique cannot be used to solve for ψ in the slot. For this reason ψ has been expressed as the superposition of three parts. Within the corner region this corresponds to

$$\psi \sim x - 1 + \psi_A + \psi_B,$$

where ψ_A is defined so that $\partial\psi_B/\partial x \to 0$ as $x \to 1$ on $z = 0$, permitting Smith's technique to be used to solve for ψ_B. It is evident from (4.10*b*) that ψ_A has been so defined.

The local forms of ψ_A and ψ_B can be identified. Since $\partial^2\psi_A/\partial z^2 \sim 0$ and

$$\frac{\partial\psi_A}{\partial x} \sim \frac{(\frac{1}{2}\pi\tan\Theta_R - 1)\sin 2\Theta_R}{\sin 2\Theta_R - 2\Theta_R},$$

on $z = 0$ as $x \to 0$, and both $\psi_A \sim 0$ and $\partial\psi_A/\partial x \sim 0$ on $x = 1$ as $z \to 0$, it can readily be verified that

$$\psi_A \sim \frac{\sin 2\Theta_R}{\sin 2\Theta_R - 2\Theta_R}(\tan\Theta_R - \tfrac{1}{2}\pi)(1-x)\arctan\frac{(1-x)}{z}. \qquad \text{(A 2)}$$

Subtracting $x-1$ and (A 2) from (A 1) gives

$$\psi_B \sim \left\{1-x+\left[\frac{2}{\pi}(1-x)-z\right]\arctan\frac{(1-x)}{z}\right\}\frac{\sin 2\Theta_R}{\sin 2\Theta_R - 2\Theta_R}.$$

Thus, we have

$$\frac{\partial^2\psi_B}{\partial z^2} \sim \frac{2}{1-x}\frac{\sin 2\Theta_R}{\sin 2\Theta_R - 2\Theta_R} \quad \text{on } z = 0,$$

and

$$\frac{\partial^2\psi_B}{\partial x^2} \sim 0 \quad \text{on } z = 0.$$

These are the limiting forms of the expressions for b_1 and b_2 on $z = 0$ as $x \to 1$ used in (4.29).

REFERENCES

ABRAMOWITZ, M. & STEGUN, I. 1964 *Handbook of Mathematical Functions with Formulas, Graphs, and Mathematical Tables.* NBS Appl. Maths Series No. 55, US Government Printing Office, Washington DC.

AUSSERE, D., PICARD, A. M. & LEGER, L. 1986 Existence and role of the precursor film in the spreading of polymer liquids. *Phys. Rev. Lett.* **57**, 2671.

BACH, P. & HASSAGER, O. 1985 An algorithm for the use of the Lagrangian specification in Newtonian fluid mechanics and applications to free-surface flow. *J. Fluid Mech.* **152**, 173.

BASCOM, W. D., COTTINGTON, R. L. & SINGLETERRY, C. R. 1964 Dynamic surface phenomena in the spontaneous spreading of oils on solids. In *Adv. Chem.: Am. Chem. Soc.* **43**, 389.

COX, R. G. 1986 The dynamics of the spreading of a liquid on a solid surface. *J. Fluid Mech.* **168**, 169.

DUSSAN V., E. B. 1976 The moving contact line: the slip boundary condition. *J. Fluid Mech.* **77**, 665.

DUSSAN V., E. B. 1979 On the spreading of liquids on solid surfaces: static and dynamic contact lines. *Ann. Rev. Fluid Mech.* **11**, 371.

DUSSAN V., E. B. & DAVIS, S. H. 1974 On the motion of a fluid–fluid interface along a solid surface. *J. Fluid Mech.* **65**, 71.

GENNES, P. G. DE 1985 Wetting: statics and dynamics. *Rev. Mod. Phys.* **57**, 827.

GOLDSTEIN, S. 1938 *Modern Developments in Fluid Dynamics*, pp. 676–680. Oxford University Press.

GREGORY, R. D. 1980*a* The semi-infinite strip $x > 0, -1 < y < 1$; completeness of the Papkovich–Fadle eigenfunctions when $\phi_{xx}(0, y), \phi_{yy}(0, y)$ are prescribed. *J. Elast.* **10**, 57.

GREGORY, R. D. 1980*b* The traction boundary-value problem for the elastostatic semi-infinite strip; existence of solution, and completeness of the Papkovich–Fadle eigenfunctions. *J. Elast.* **10**, 295.

HANSEN, R. J. & TOONG, T. Y. 1971 Dynamic contact angle and its relationship to forces of hydrodynamic origin. *J. Colloid Interface Sci.* **37**, 196.

HARDY, W. B. 1919 The spreading of liquids on glass. *Philos. Mag.* **38**, 49.

HOCKING, L. M. 1976 A moving fluid interface on a rough surface. *J. Fluid Mech.* **76**, 801.

HOCKING, L. M. 1977 A moving fluid interface. Part 2. The removal of the force singularity by a slip flow. *J. Fluid Mech.* **77**, 209.

HOCKING, L. M. 1981 Sliding and spreading of two-dimensional drops. *Q. J. Mech. Appl. Maths* **34**, 37.

HOCKING, L. M. 1983 The spreading of a thin drop by gravity and capillary. *Q. J. Mech. Appl. Maths* **36**, 55.

HOCKING, L. M. & RIVERS, A. D. 1982 The spreading of a drop by capillary action. *J. Fluid Mech.* **121**, 425.

HUH, C. & MASON, S. G. 1977 The steady motion of a liquid meniscus in a capillary tube. *J. Fluid Mech.* **81**, 401.

JACKSON, R. 1977 *Transport in Porous Catalysts.* Elsevier.

JANSONS, K. M. 1986 Moving contact lines at non-zero capillary number. *J. Fluid Mech.* **167**, 393.

JANSONS, K. M. 1988 Determination of the macroscopic (partial) slip boundary condition for a viscous flow over a randomly rough surface with a perfect slip boundary condition microscopically. *Phys. Fluids* **31**, 15.

JOSEPH, D. D. 1977 The convergence of biorthogonal series for biharmonic and Stokes flow edge problems. Part I. *SIAM J. Appl. Maths* **33**, 337.

JOSEPH, D. D. & STURGES, L. 1975 The free surface on a liquid filling a trench heated from its side. *J. Fluid Mech.* **69**, 565.

JOSEPH, D. D. & STURGES, L. 1978 The convergence of biorthogonal series for biharmonic and Stokes flow edge problems. Part II. *SIAM J. Appl. Maths* **34**, 7.

JOSEPH, D. D., STURGES, L. & WARNER, W. H. 1982 Convergence of biorthogonal series of biharmonic eigenfunctions by the method of Titchmarsh. *Arch. Rat. Mech.* **78**, 223.

KAFKA, F. Y. & DUSSAN V., E. B. 1979 On the interpretation of the dynamic contact angles in capillaries. *J. Fluid Mech.* **95**, 539.

LOWNDES, J. 1980 The numerical simulation of the steady motion of the fluid meniscus in a capillary tube. *J. Fluid Mech.* **101**, 631.

NGAN, C. G. 1985 An assessment of the proper modelling assumptions for the spreading of liquids on solid surfaces. PhD thesis, University of Pennsylvania.

NGAN, C. G. & DUSSAN V., E. B. 1982 On the nature of the dynamic contact angle: an experimental study. *J. Fluid Mech.* **118**, 27.

NGAN, C. G. & DUSSAN V., E. B. 1984 The moving contact line with a 180 degree advancing contact angle. *Phys. Fluids* **27**, 2785.

PISMEN, L. M. & NIR, A. 1982 Motion of a contact line. *Phys. Fluids* **25**, 3.

RICHARDSON, S. 1973 On the no-slip boundary condition. *J. Fluid Mech.* **59**, 707.

ROSE, W. & HEINS, R. W. 1962 Moving interfaces and contact angle rate-dependence. *J. Colloid Interface Sci.* **17**, 39.

SMITH, R. C. T. 1952 The bending of a semi-infinite strip. *Austral. J. Sci. Res.* A **5**, 227.

WHITE, C. 1983 Integration of stiff differential equations in chemical reactor modelling. PhD thesis, University of Pennsylvania.